# Aerosol ultraviolet absorption experiment (2002 to 2004), part 2: absorption optical thickness, refractive index, and single scattering albedo

**Nickolay Krotkov**
University of Maryland
Goddard Earth Sciences and Technology Center
Baltimore County, Maryland 21228
E-mail: Krotkov@chescat.gsfc.nasa.gov

**Pawan K. Bhartia**
**Jay Herman**
NASA Goddard Space Flight Center
Greenbelt, Maryland 20771

**James Slusser,** MEMBER SPIE
**Gwendolyn Scott**
Colorado State University
Natural Resources Ecology Laboratory
U.S. Department of Agriculture
UV-B Monitoring and Research Network
Fort Collins, Colorado 80523

**Gordon Labow**
**Alexander P. Vasilkov**
Science Systems and Appliations, Inc.
Lantham, Maryland 20706

**Thomas F. Eck**
**Oleg Dubovik**
University of Maryland
Goddard Earth Sciences and Technology Center
Baltimore County, Maryland 21228

**Brent N. Holben**
NASA Goddard Space Flight Center
Greenbelt, Maryland 20771

**Abstract.** Compared to the visible spectral region, very little is known about aerosol absorption in the UV. Without such information it is impossible to quantify the causes of the observed discrepancy between modeled and measured UV irradiances and photolysis rates. We report results of a 17-month aerosol column absorption monitoring experiment conducted in Greenbelt, Maryland, where the imaginary part of effective refractive index $k$ was inferred from the measurements of direct and diffuse atmospheric transmittances by a UV-multifilter rotating shadowband radiometer [UV-MFRSR, U.S. Department of Agriculture (USDA) UV-B Monitoring and Research Network]. Colocated ancillary measurements of aerosol effective particle size distribution and refractive index in the visible wavelengths [by CIMEL sun-sky radiometers, National Aeronautics and Space Administration (NASA) Aerosol Robotic Network (AERONET)], column ozone, surface pressure, and albedo constrain the forward radiative transfer model input, so that a unique solution for $k$ is obtained independently in each UV-MFRSR spectral channel. Inferred values of $k$ are systematically larger in the UV than in the visible wavelengths. The inferred $k$ values enable calculation of the single scattering albedo $\omega$, which is compared with AERONET inversions in the visible wavelengths. On cloud-free days with high aerosol loadings [$\tau_{ext}(440) > 0.4$], $\omega$ is systematically lower at 368 nm ($\langle\omega_{368}\rangle = 0.94$) than at 440 nm ($\langle\omega_{440}\rangle = 0.96$), however, the mean $\omega$ differences (0.02) are within expected uncertainties of $\omega$ retrievals ($\sim$0.03). The inferred $\omega$ is even lower at shorter UV wavelengths ($\langle\omega_{325}\rangle \sim \langle\omega_{332}\rangle = 0.92$), which might suggest the presence of selectively UV absorbing aerosols. We also find that $\omega$ decreases with decrease in aerosol loading. This could be due to real changes in the average aerosol composition between summer and winter months at the Goddard Space Flight Center (GSFC) site. Combing measurements of $\tau_{ext}$ and $\omega$, the seasonal dependence of the aerosol absorption optical thickness, $\tau_{abs} = \tau_{ext}(1-\omega)$ is derived in the UV with an uncertainty of 0.01 to 0.02, limited by the accuracy of UV-MFRSR measurement and calibration. The $\tau_{abs}$ has a pronounced seasonal dependence with maximum values $\sim$0.1 occurring in summer hazy conditions and $<$0.02 in the winter and fall seasons, when aerosol loadings are small. The measured $\tau_{abs}$ is sufficient to explain both the magnitude and seasonal dependence of the bias in satellite estimates of surface UV irradiance previously seen with ground-based UV measurements.
 [DOI: 10.1117/1.1886819]

Subject terms: ultraviolet radiation; aerosol absorption; single scattering albedo; CIMEL sunphotometer; AERONET network; ultraviolet multifilter rotating shadowband radiometer; diffuse fraction measurements.

Paper UV-11 received Apr. 14, 2004; revised manuscript received Dec. 15, 2004; accepted for publication Jan. 24, 2005; published online Apr. 8, 2005.

## 1 Introduction

Aerosols in the boundary layer can significantly change air quality either directly or by affecting the rate of tropospheric ozone (urban smog) formation.[1–4] Scattering by aerosols increases the actinic flux and the rates of photochemical reactions in the upper parts of the planetary boundary layer,[1–6] while aerosol absorption reduces the amount of UV radiation available for chemical reactions within and below the aerosol layer.[1–5] Therefore, without accurate knowledge of aerosol UV absorption (or single-scattering albedo) the magnitude and even the sign of the aerosol effect on tropospheric photochemistry remain highly uncertain.[1–6] By the same reasoning, the boundary layer aerosol absorption uncertainty remains a serious obstacle in satellite estimation of biologically harmful UV

0091-3286/2005/$22.00 © 2005 SPIE

irradiance at the surface.[7–13] Although it is well known that iron oxides in desert dust[14–16] and soot produced by fossil fuel burning and urban transportation[17–21] strongly absorb UV radiation, properties of other potential UV absorbers, e.g., organic and nitrated and aromatic aerosols,[22,23] are poorly known. In addition, different aerosol components are often mixed in an atmospheric column downwind from urban regions.[24] This makes it difficult to quantify aerosol effects on UV irradiance and photolysis rates from the models. On the other hand, ground-based passive remote sensing techniques enable estimation of column aerosol absorption without prior knowledge of aerosol composition. The techniques are based on nearly simultaneous measurements of direct sun irradiance and diffuse sky radiance[25–28] or irradiance,[29–34] from which column average absorption can be inferred (with aircraft measurements providing vertically resolved information[21,24]). The multiyear mean column aerosol absorption climatology in the visible has been established for several sites using CIMEL almucantar inversions[25–27] from the global Aerosol Robotic Network (AERONET) network,[35,36] but these inversions are not yet available at UV wavelengths. Ground-based remote measurements of aerosol UV absorption were also demonstrated,[37–42] but these retrievals have not been validated. Neither technique has yet enabled deriving seasonal aerosol absorption climatology.

To validate column aerosol absorption retrievals in the UV and produce a long-term seasonal data set of aerosol column absorption optical thickness $\tau_{abs}$ a UV multifilter rotating shadowband radiometer[43,44] (UV-MFRSR, Yankee Environmental Systems, Turners Falls, Massachusetts) and a rotating triad of sun-sky CIMEL radiometers [reference instruments of the National Aeronautics and Space Administration (NASA) AERONET network[35,36]] were run side-by-side continuously for 17 months at the NASA Goddard Space Flight Center in Greenbelt, Maryland. A previous paper[45] showed that the AERONET data could be used for UV-MFRSR daily on-site calibration and accurate measurements of $\tau_{ext}$ at three UV-A wavelength channels. The essential advantage of the schadowband technique[29–34] is that calibration obtained for direct-sun voltage can be directly applied to obtain diffuse atmospheric transmittance.[43,45] The transmittance combined with accurate $\tau_{ext}$ data and a radiative transfer model enables the aerosol absorption and single scattering albedo retrievals described in this paper. The paper is organized as follows. Section 2 describes briefly the data sets used in this study. Section 3 provides a description of the UV-MFRSR inversion technique implementation, and Sec. 4 discusses aerosol absorption results and comparisons with AERONET inversion data in the visible wavelengths. Section 5 discusses application of the aerosol UV absorption optical thickness data to explain the bias in satellite surface-UV estimates. A sensitivity study and accuracy assessments of the aerosol UV absorption retrievals are discussed in the appendix (Sec. 7).

## 2 Data Sets

The primary data set consists of 3-min measurements of diffuse and total irradiance collected with the UV-MFRSR instrument[43,44] (optical head 271) from the U.S. Department of Agriculture (USDA) UV-B Monitoring and Research Network[46] (UVMRP). A single measurement cycle consisted of measuring total horizontal irradiance (no sun blocking) followed by three irradiance measurements with different positions of the shadowband blocking the sun and sky radiance on each side of the sun (at 9 deg). All spectral channels were measured within 1 s by seven separate solid state detectors with interference filters sharing a common Teflon diffuser.[43] The complete shadowing cycle took ~10 s and was repeated every 3 min throughout the day without averaging of the data. The raw data (voltages) were automatically transmitted every night (via dedicated telephone modem) to the USDA UVMRP processing center at the Colorado State University (Fort Collins) for voltage corrections and further processing. The standard UVMRP calibration procedure differs from that used in our experiments, where we used only cosine-corrected voltages calibrated on-site against our colocated reference AERONET sunphotometers. This method yields more accurate measurements of $\tau_{ext}$ and diffuse and direct atmospheric transmittances. A detailed description of the UV-MFRSR operating procedures, raw voltage corrections, and on-site calibration procedure was a subject of our first paper[45] (this issue), therefore, only a brief summary is provided here.

### 2.1 *Direct and Diffuse Transmittances*

In addition to UV-MFRSR data, $\tau_{ext}$ was continuously measured with a rotating triad of CIMEL radiometers that were reference instruments of the AERONET global network[35,36] (data available at http://aeronet.gsfc.nasa.gov). The automatic tracking sun- and sky-scanning radiometers made direct sun measurements with a 1.2-deg full field of view every 15 min at 340, 380, 440, 500, 675, 870, 940, and 1020 nm (accuracy typically[35,36,47] ~0.003 to 0.01 in the visible with larger errors in the UV). The pressure-corrected $\tau_{ext}$ at 340 and 380 nm and the standard $\tau_{ext}$ at 440 and 500 nm were interpolated in time and wavelength and compared with the UV-MFRSR measurements of cosine-corrected direct-normal voltages to derive a more accurate daily $V_0$ calibration[45] than provided in the standard UVMRP data set[48] (http://uvb.nrel.colostate.edu). The derived $V_0$ for each spectral channel agreed with those from Langley UV-MFRSR measurements obtained on completely cloud free days.[45] The improved calibration was used to obtain both direct ($T_R$) and diffuse ($T_D$) atmospheric transmittances with high accuracy (2 to 4% at 368 nm, see Table 4 in the appendix).

### 2.2 *Surface Pressure and Total Ozone Measurements*

Accurately specifying surface pressure is an important requirement for radiation modeling in the UV spectral region. Surface pressure measurements at a nearby (5 km away) USDA location in Beltsville, Maryland, were used reduced by ~2 mbar to account for change in altitude between Beltsville location [~70 m above sea level (ASL)] and GSFC UV-MFRSR location [roof of the building, ~90 m ASL according to our global positioning system (GPS) measurements[45]].

Ancillary measurements at our site included Brewer double-monochromator column ozone measurements. Missing Brewer ozone measurements were filled in with the Earth Probe/Total Ozone Mapping Spectrometer

(EP/TOMS) total ozone data, since both ozone data sets agreed quite well (within 2%). The ozone values were used to calculate ozone absorption optical thickness, $\tau_{O3}$ in each UV-MFRSR spectral channel for each individual measurement. The pressure measurements were used (1) to calculate accurate Rayleigh scattering optical thickness $\tau_R$ and (2) to correct standard AERONET aerosol $\tau_{\text{ext}}$ at 340- and 380-nm data used for calibration (see Sec. 2.1).

### 2.3 *Aerosol Extinction Optical Thickness*

Daily average $V_0$ estimates along with $\tau_R$ and $\tau_{O3}$ were used to calculate aerosol $\tau_{\text{ext}}$ for individual UV-MFRSR measurements.[45] The 3-min UV-MFRSR $\tau_{\text{ext}}$ data compared well with interpolated 15-min AERONET $\tau_{\text{ext}}$ measurements with only a small scatter [at 368-nm daily root mean square (rms) differences between AERONET and UV-MFRSR $\tau_{\text{ext}}$ were within 0.01 ($1\sigma$)] on all cloud-free days. This analysis[45] has shown that the UV-MFRSR, when intercalibrated against an AERONET sunphotometer on the same day, was proven reliable to retrieve $\tau_{\text{ext}}$.

With $\tau_{\text{ext}}$ known, the only radiative transfer (RT) model input parameters are surface albedo $A$, aerosol phase function (average cosine, $g$), and single scattering albedo $\omega$. For $\omega$ to be inferred by means of fitting of calculated and measured transmittances, $A$ and $g$ were to be estimated from ancillary measurements as described in the following.

### 2.4 *Aerosol Phase Function and Asymmetry Parameter*

CIMEL sky radiance almucantar measurements at 440, 675, 870, and 1020 nm (downloaded from the website http://aeronet.gsfc.nasa.gov) were used in conjunction with $\tau_{\text{ext}}$ at these wavelengths to retrieve column average particle size distribution (PSD) and effective refractive index [real ($n$) and imaginary ($k$), independently at each of the noted wavelengths] following methodology of Dubovik and King[25] and Dubovik et al.[26,27] Even though it is well known that dustlike particles have irregular shapes arising from the fracturing of larger grains, the AERONET retrieval assumes the aerosol particles to be polydisperse homogeneous spheres that have the same complex refractive index. Sensitivity studies by Dubovik et al.[26] examined how much these assumptions mislead the inversion solutions in the cases of nonspherical dust aerosols and in the case of nonhomogenous aerosols (externally or internally mixed spherical particles with different refractive indices). For all tested cases, no significant errors where observed in the retrieval of a single scattering albedo, which is the focus of our study.

The aerosol phase functions at UV-MFRSR wavelengths were calculated using the AERONET PSD and refractive index at 440 nm (real part) inversions within 60 min of each UV-MFRSR measurement using forward Mie calculations, as described in Sec. 3.

### 2.5 *Surface Albedo*

It was previously shown that changes in $A$ from 0.4 to 0.8 result in a 30% increase in diffuse atmospheric transmittance.[29–31] However, in the UV spectral region, $A$ is only a few percent for snow-free terrain, therefore, climatological values are usually acceptable.[49] Excluding days with traces of partial snow cover enabled us to use TOMS-derived climatologically snow-free values of surface albedo.[49] Low surface albedo in UV-A$\sim$0.02 at the Goddard Space Flight Center (GSFC) site was confirmed from satellite overpass 360-nm reflectivity measurements from the EP/TOMS on clear snow-free days (http://toms.gsfc.nasa.gov). Such low values of surface albedo provide an important advantage for measuring aerosol properties in the UV spectral range. Maximum possible deviations $\sim$0.02 in $A$ from the assumed climatological value ($A=0.02$) would result in 1.5% changes in the diffuse irradiance transmittance and even smaller changes in total transmittance and diffuse fraction ratio.

### 2.6 *Aerosol Vertical Distribution*

The aerosol vertical distribution was shown to be not important for aerosol absorption determination (see later discussion in Sec. 4). Therefore, a fixed exponential aerosol vertical profile in the lower troposphere was used in the forward model with no stratospheric aerosol.

With $\tau_{O3}$, $\tau_R$, $\tau_{\text{ext}}$, $A$, and $g$ predetermined in each UV-MFRSR channel, the only free RT model input parameter is single scattering albedo $\omega$. Therefore, $\omega$ was inferred with a forward RT model by requiring that calculated transmittances (or their ratios) match the measured ones (Sec. 2.1) independently in each UV-MFRSR channel. Technically, Mie calculations were incorporated in the forward model to account for $g$ spectral dependence without using look-up tables. The details are given in Sec. 3.

## 3 UV-MFRSR Aerosol Absorption Inversion Technique

Only UV-MFRSR data corresponding to horizontally homogeneous cloud-free atmospheric conditions were used. The cloud-free portions of days were selected by visual examination and analysis of 3-min irradiance series and all-sky camera images.

The fitting to the forward model was done separately for different transmittances and their ratios [the diffuse-to-direct ratio[29–31] ($D_D=T_D/T_R$), the diffuse fraction[32–34] ($D_T=T_D/T_T$), and the total transmittance[7] ($T=V_T/V_0$)] at each UV-MFRSR spectral channel. The advantage of utilizing dimensionless ratios ($D_D$, $D_T$, and $T$) is that absolute radiometric calibration is not required, since the same detector measures both the total and diffuse flux.[43] Agreement between all three methods provides a robust check on relative UV-MFRSR spectral calibration and the correction for systematic measurement errors (i.e., angular and spectral response corrections[45]).

To obtain the UV-MFRSR aerosol inversions, CIMEL almucantar measurements and $\tau_{\text{ext}}$ were used[25–27] (Sec. 2.4). Each alumcantar measurement took 5 minutes and was repeated every hour and direct sun $\tau_{\text{ext}}$ measurement was repeated every 15 min (Sec. 2.3). All available UV-MFRSR data (every 3 min) within time interval $\pm$60 min of each AERONET almucantar measurement were analyzed. Our assumption was that the aerosol type did not change during this period and that observed changes in the radiation field arise from changes in solar zenith angle and aerosol optical thickness. Therefore, we used the same aerosol size distribution and the real part of refractive index

within each 60-min time slot, but allowed for $\tau_{ext}$ and $\theta_0$ changes in 3-min increments using UV-MFRSR measurements. If the time slots for two consecutive AERONET retrievals overlapped, we repeated the UV-MFRSR fitting for all overlapping points with the new aerosol parameters. This provided a test of sensitivity of our results to real-time changes in the AERONET inversion parameters (PSD and $n_R$) used as input to our fitting technique. Forward RT calculations were run to fit every single 3-min UV-MFRSR measurement independently at each wavelength. The advantage of this approach is that forward RT calculations were always done for the exact values of solar zenith angle, $\tau_{ext}$, and aerosol parameters. The methodology of forward modeling and $\omega$ retrieval was as follows:

1. Standard discrete AERONET column volume PSD in 22 size bins between 0.05 and 15 $\mu$m were fit using a bimodal lognormal volume size distribution.[27] This parameterization requires six input parameters: column volume, modal radius, and standard deviation separately for fine and coarse modes.
2. Volume PSD parameters were analytically converted to the column number density parameters required as input to the Mie code.[50] Since only the shape of the PSD was required, five input parameters remained: modal radii and standard deviations separately for fine and coarse modes and the ratio of the total number of particles in fine and course modes. The implicit PSD normalization occurs by requiring the model input $\tau_{ext}$ equal to the UV-MFRSR measured $\tau_{ext}$.
3. In our Mie code, the refractive index was assumed to be the same for fine and coarse modes (one component aerosol model) to be consistent with AERONET inversions.[25–27] Thus, following current AERONET assumptions, a single optically effective refractive index was retrieved, which was a weighted mean of the true column average refractive index over the particle size distribution.
4. The real part of refractive index $n$ was assumed to be constant with wavelength, and was fixed to the AERONET retrieved value at 440 nm. This approximation was possible, since the direct transmittance was forced to be equal to the measured one through the independently measured $\tau_{ext}$, while diffuse irradiance only weakly depends on the real part of refractive index.[29–31]
5. An *a priori* vertical profile of the aerosols, which peaks in the boundary layer, was assumed in our forward model. The additional assumption was that neither aerosol PSD nor the refractive index change with altitude, which was consistent with AERONET inversions.[25–27] No stratospheric aerosol was assumed.
6. In the forward RT model, the TOMS climatological ozone and temperature profiles were used that were scaled to the Brewer measured total column ozone amount for every UV-MFRSR measurement. The Brewer total ozone amount compared well with TOMS ozone measurements so that TOMS ozone values could be used to fill in days with missing Brewer ozone measurements. No gaseous absorption other than ozone was assumed.
7. The ancillary measurements available at GSFC location (see Sec. 2) enabled us to constrain all required input to the Mie scattering code within the forward RT model, except the imaginary part of the aerosol refractive index $k$, which is related to effective column aerosol absorption. The $k$ was inferred by fitting either diffuse to direct ($DD=V_F/V_D$) or diffuse fraction ($D_T=V_F/V_T$) or total transmittance ($T=V_T/V_0$) measurements to the RT calculated values separately in each spectral channel. The fitting was done iteratively starting with AERONET derived $k_{440}$ as the initial value. The absolute value of the fitting residual was used as a measure of the goodness of the fit.
8. If a good fit was achieved, the $k(\text{fit})$ was treated as an optically effective fitting parameter, rather than microphysical particle property, because it accounts for all assumptions in the forward model as well as systematic measurement errors. The fitted value of $k(\text{fit})$, along with the AERONET PSD and $n_{440}$, were used to calculate single scattering albedo $\omega(\text{fit})$ using Lorentz-Mie code and $\tau_{abs}=[1-\omega(\text{fit})]\tau_{ext}$. Derived radiative properties ($\omega, \tau_{abs}$) were less dependent on model assumptions so that their errors were smaller than errors in $k$ (see the appendix for estimation of errors).
9. As an independent check, we estimated the diffuse fraction by varying $\omega$ directly as an input parameter to a different RT code [the tropospheric UV-visible 4 (TUV4, Ref. 6), based on the discrete ordinate radiative transfer[51] (DISORT) code]. Both $\omega$ retrievals agreed well (within 0.01) at 368 nm, provided that the CIMEL-derived value of the asymmetry parameter $g_{368}$ was used as input to the TUV model. This check provides confidence that Mie model assumptions and forward RT calculations were not a major source of error in the retrievals of $\omega$ and $\tau_{abs}$.

## 4 UV-MFRSR Retrieval Results

The inferred values of $k$ and $\omega$ in the UV wavelengths were used (1) to compare with independent AERONET $\omega$ (Sec. 4.1) and $k$ (Sec. 4.2) retrievals at 440 nm and (2) to infer seasonal dependence of aerosol absorption optical thickness, $\tau_{abs}=\tau_{ext}(1-\omega)$ (Sec. 4.3). The comparison data set was limited because of the following conditions. Completely cloud-free periods were manually selected (using visual sky observations) that coincided with UV-MFRSR calibration periods.[45] Days with partial snow cover were manually filtered out, with ~100 cloud-free portions of days remained between October 1, 2002, and March 25, 2004, meeting our cloud-free and snow-free criteria. To compare only high-quality $\omega$ and $k$ retrievals, only the inversions with $\tau_{ext}(440\,\text{nm})>0.4$ and solar zenith angle $\theta_0>45$ deg (required for good AERONET inversions[25–27]) and $\theta_0<70$ deg (required for good UV-MFRSR inversions to minimize cosine correction errors[45]) were selected.

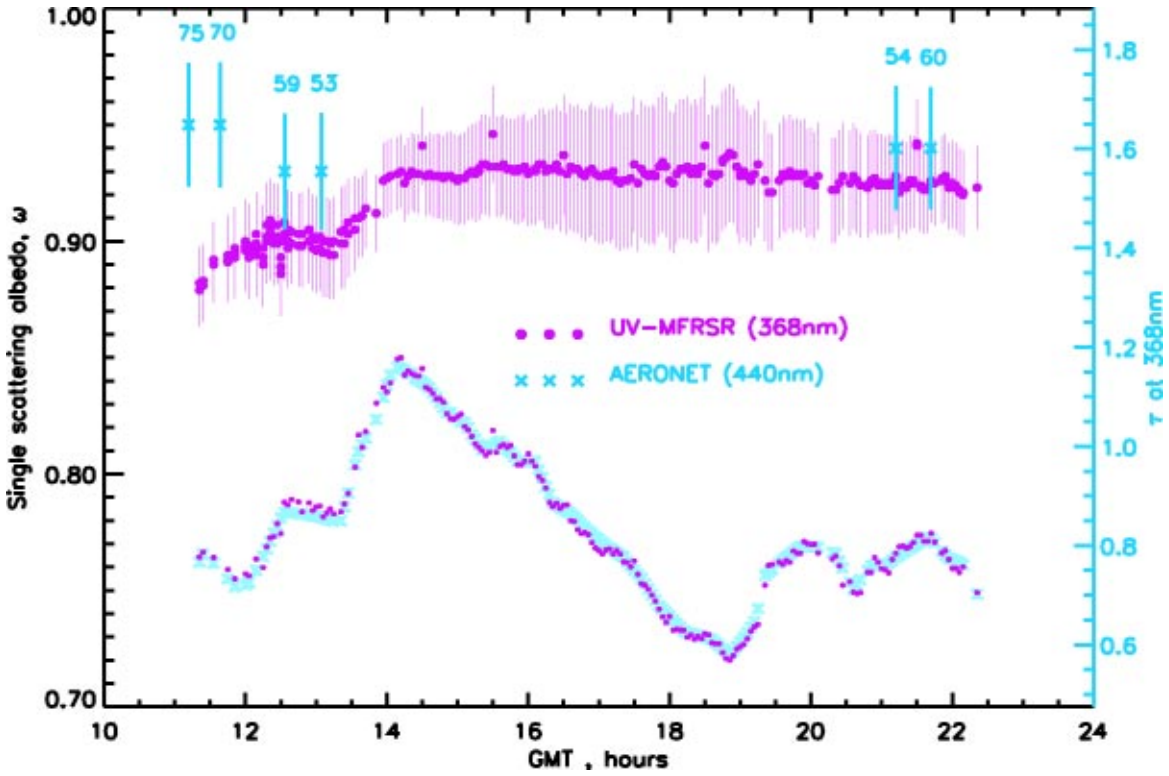


**Fig. 1** UV-MFRSR and AERONET single-scattering albedo retrieval at GSFC on June 2, 2003. The 3-min UV-MFRSR retrieved single-scattered albedos at 368 nm are shown as small spheres, while AERONET $\omega_{440}$ retrievals at 440 nm are shown as large crosses with $\pm 0.03$ error bars.[26] The actual solar zenith angle was used in retrieval for each 3-min UV-MFRSR measurement. The UV-MFRSR assumptions were surface albedo of 0.02, Brewer-measured total ozone, and boundary layer aerosol profile and Dubovik and King[25] inverted particle size distribution within $\pm 60$ min of each CIMEL almucantar measurement. In addition, $\tau_{ext}$ at 368 nm is shown for both instruments (same symbols) with right axis scale.

For all cases, UV-MFRSR data were processed three times using different measured fitting parameters (diffuse/direct voltage ratio, diffuse/total voltage ratio, and total normalized transmittance $V_T/V_0$). All three methods provided consistent inversion results (within 0.01 in $\omega$). As an additional check, the comparisons were made with $\omega$ retrievals using a different forward RT code [TUV (Ref. 6)]. The retrievals were essentially the same ($\omega$ within 0.01) when the correct $g$ factor was used in the forward model [TUV (Ref. 6)]. Selected $\omega$ comparison cases are shown in Figs. 1 to 3.

### 4.1 *Single Scattering Albedo*

Figure 1 shows $\omega$ retrievals by both instruments on June 2, 2003, when a long-range smoke plume was moving over GSFC location. The passage of the plume was evident from enhanced extinction optical thickness $\tau_{368}$ measured by both instruments (shown on the right axis in Fig. 2). Visually, horizontal visibility remained high on this day with clear sight of horizon; however, the sky color was unusually white. According to the 3-min UV-MFRSR data, the most absorbing part of the smoke plume ($\omega_{368} \sim 0.88$ to 0.9) was recorded in the morning [<14 Universal Time (UT), also Greenwich Mean Time (GMT)] with less absorbing $\omega_{368} \sim 0.93$ for the rest of the day. Back trajectory analysis and satellite data suggested that the smoke plume was originated from fires in Siberia near lake Baikal. Physical-chemical processes during long-range transport of smoke can explain this relatively low absorption. Boreal forest smoke typically does not have low $\omega$ due to significant particle production from smoldering of woody fuels, which yields relatively small black carbon percentages. Also smoke particles tend to become less absorbing with age as the particle size increases due to coagulation during transport.[52] The Angström exponent was high and stable during the day ($\alpha_{440/870} = 1.73$ to 1.88), suggesting predominantly fine-mode particles. However, the Angström exponent was smaller in the UV ($\alpha_{380/440} = 0.73$ to 0.82) compared to the visible wavelengths. This suggests substantial curvature of the $\ln(\tau)$ versus $\ln(\lambda)$ dependence ($\alpha' = 1.7$ to 1.8).[47] The cause of large $\omega$ discrepancy in the morning ($\sim$11.5 UT) remains unknown.

Although complete AERONET inversions were available for the whole day, $\omega_{440}$ retrievals were not shown for solar zenith angles less than 45 deg, because the uncertainty in $\omega_{440}$ is significantly larger for these cases.[26,27] However, AERONET inverted particle size distribution results were shown to be accurate for all conditions,[26,27] and they are used for UV-MFRSR retrievals without restriction on solar elevation. On the other hand, UV-MFRSR $\omega_{368}$ retrievals were not shown for high solar zenith angle cases when $\theta_0 > 75$ deg, because the cosine-correction uncertainty for the

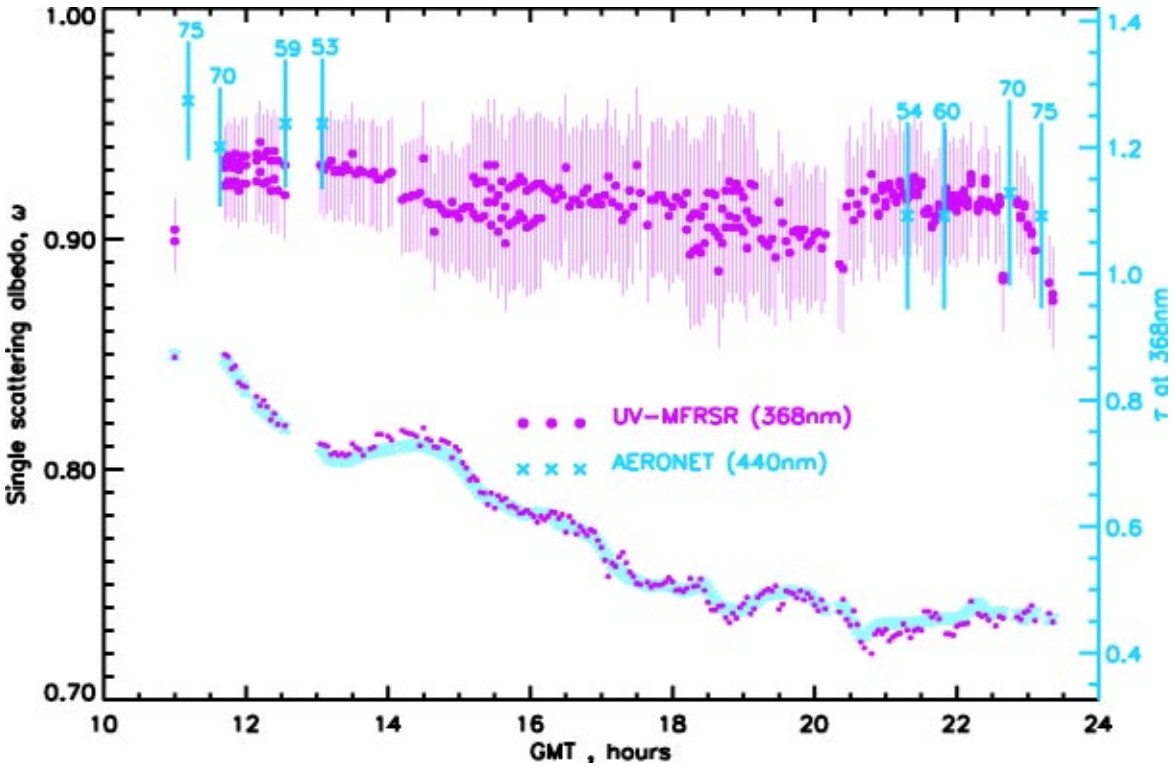


**Fig. 2** UV-MFRSR and AERONET $\omega$ retrieval at GSFC on June 24, 2003. The 3-min UV-MFRSR $\omega_{368}$ is shown as small spheres, while AERONET $\omega_{440}$ retrievals are shown as large crosses with $\pm 0.03$ error bars.[27] In addition, $\tau_{ext}$ at 368 nm is shown for both instruments (same symbols) with right axis scale. The actual solar zenith angle was used in retrieval for each 3-min UV-MFRSR measurement. The UV-MFRSR assumptions were $A=0.02$, Brewer-measured total ozone, boundary layer aerosol profile, and AERONET inverted[25] particle size distribution within $\pm 60$ min of each CIMEL almucantar measurement.

measured diffuse irradiance is larger for these cases.[45] The additional uncertainty at high solar zenith angles arises from using a pseudospherical version of the forward radiative transfer code, which corrects only direct sun irradiance, thus underestimating diffuse irradiance.[50] Thus, the two methods of estimating $\omega$ are complementary in that the AERONET retrieval[25–27] requires large solar angles, while UV-MFRSR data are more reliable at low solar zenith angles.

The real part of refractive index at 440 nm, $n_{440}$, increased from 1.39 to 1.5 during smoke passage and decreased later to 1.46. The imaginary part of refractive index was systematically higher in UV than in the visible ($k_{368}=0.014$ to 0.02, $k_{440}=0.007$ to 0.013). The difference was larger than specified uncertainty for AERONET $k$ retrievals[27] ($\pm 0.003$) for all cases except one retrieval. These differences in $k$ were consistent with lower $\omega$ values in UV ($\omega_{368}=0.89$ to 0.92 compared to $\omega_{440}=0.93$ to 0.95). This suggests that $\omega$ spectral dependence in the visible (lower $\omega$ at longer wavelengths[27]) flattens out and even reverses in the UV. However, it is emphasized that, except for solar zenith angles larger than 70 deg, the $\omega$ retrieved at 368 and 440 nm are within the range of overlap of both retrieval uncertainties.

The sensitivity of $\omega_{368}$ results to assumed aerosol vertical profile was also studied. The smoke plume height over Eastern Shore in Maryland and Virginia was $\sim 3$ km according to lidar data [University of Maryland Baltimore County (UMBC) elastic lidar system (ELF) at Chesapeake Lighhouse, 36°54.6′N, 75°42.6′W). Therefore, UV-MFRSR retrievals were repeated with aerosol height at 3 km with essentially unchanged $\omega$ results. Therefore it was concluded that UV-MFRSR results were not sensitive to the smoke vertical profile (at least at 368 nm).

Figure 2 shows $\omega$ comparisons on June 24, 2003, which was typical for a summer regional ozone pollution episode. A high-pressure system over the Mid-Atlantic region for this week prevented air exchange; therefore tropospheric ozone pollution was building up as a result of local pollution (mostly traffic) and high solar irradaince[5] (air quality public warning was ''Code orange'' on this day). The conditions were mostly cloud-free for the whole day. In the morning, aerosol absorption was higher in the UV, but differences were not significant. Aerosol extinction decreased during the day, while absorption increased slightly, but more rapidly in the visible. In the afternoon, both $\omega$ retrievals were in agreement ($\omega_{368}=0.91$ to 0.92 and $\omega_{440}=0.91$ to 0.92). The AERONET inverted real part of refractive index at 440 nm changed between 1.39 and 1.59. The Ångström exponent was much higher than for smoke event on June 2, especially in the UV due to significantly smaller radius and broader $\sigma$ of the fine mode on June 24.

Strong daily variation in $\omega_{368}$ was detected on August 25, 2003 (Fig. 3), with unusually low values ($\omega_{368}\sim 0.85$)

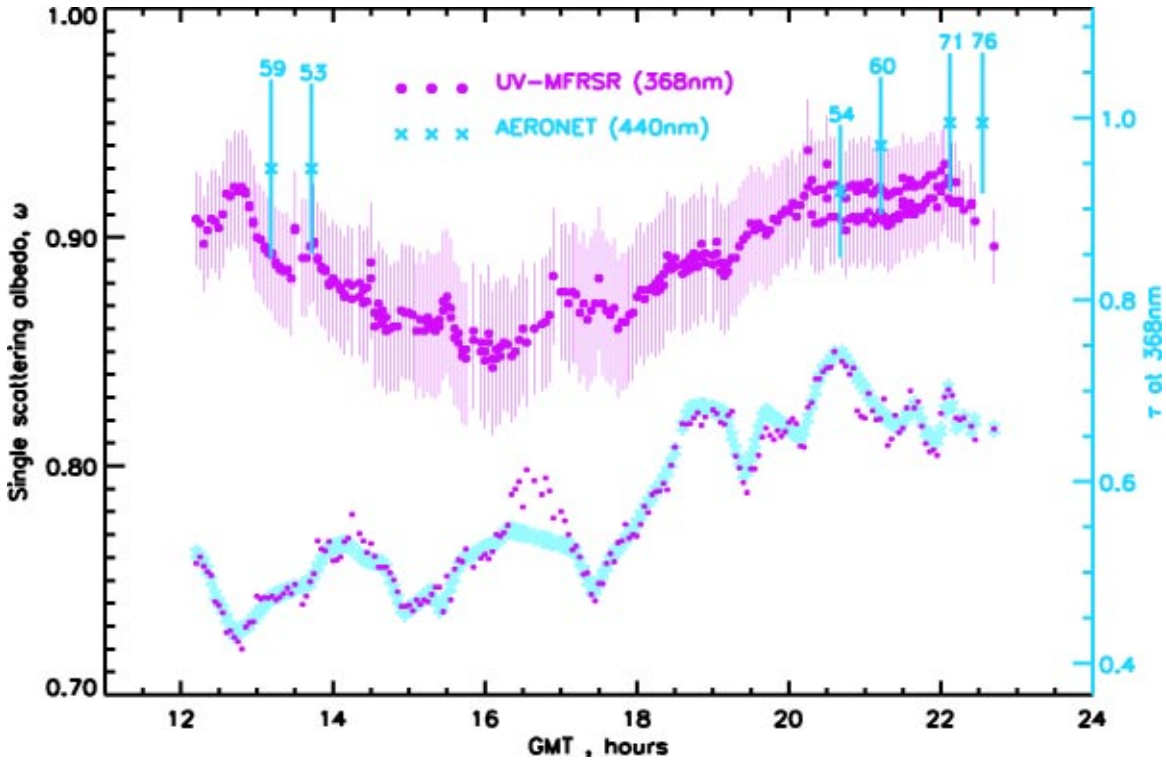


**Fig. 3** UV-MFRSR and AERONET $\omega$ retrieval at GSFC on August 25, 2003. The 3-min UV-MFRSR $\omega_{368}$ is shown as small spheres, while AERONET $\omega_{440}$ retrievals are shown as large crosses with $\pm 0.03$ error bars.[27] In addition, $\tau_{\text{ext}}$ at 368 nm is shown for both instruments (same symbols) with right axis scale. The actual solar zenith angle was used in retrieval for each 3-min UV-MFRSR measurement. The UV-MFRSR assumptions were surface albedo of 0.02, Brewer-measured total ozone, and boundary layer aerosol profile and AERONET inverted[25] particle size distribution within $\pm 60$ min of each CIMEL almucantar measurement.

in the middle of the day. This case highlights the importance of measuring the complete diurnal cycle of summertime aerosol absorption, not just morning and afternoon periods.

This case also illustrates the sensitivity of UV-MFRSR retrievals to the real part of refractive index. As was mentioned in Sec. 3, AERONET inversions of PSD and refractive index (real part at 440 nm, $n_{440}$) within 60 min of the individual UV-MFRSR measurement were used as input to the UV-MFRSR forward RT model. If the time slots for two consecutive AERONET retrievals overlap, as in case of UV-MFRSR retrievals between 20.67 and 21.2 UT, the UV-MFRSR inversions were repeated for all overlapping points with the new set of AERONET input aerosol parameters (i.e., using 21 UT retrieval in Fig. 3). In this particular example, PSDs were close for two consecutive AERONET retrievals [$R_{V,\text{fine}}=0.14\,\mu$m, $\ln(\sigma_{\text{fine}})=0.38$ at $\sim$20.67 UT versus $R_{V\,\text{fine}}=0.15\,\mu$m, $\ln(\sigma_{\text{fine}})=0.38$ at $\sim$21.2 UT], but $n_{440}$ increased significantly (from 1.33 to 1.56), causing $g_{368}$ to decrease for the latter AERONET retrieval ($g_{368}=0.735$ using $n_{440}=1.33$ at $\sim$20.5 UT and $g_{368}=0.676$ using $n_{440}=1.56$ at $\sim$21 UT).

The effect of changing $g$ on fitted $\omega$ can be understood using a two-stream approximation:[53]

$$T_T(\text{calc}) \cong 1 - \frac{(1-g_{368})\tau_{\text{ext}}}{(1-g_{368})\tau_{\text{ext}} + 2\mu_0}. \quad (1)$$

According to Eq. (1) the decrease in $g_{368}$ (meaning less asymmetric phase function) would cause calculated $T_T(\text{calc})$ to decrease with fixed $\tau_{\text{ext}}$ and solar zenith angle [$\mu_0=\cos(\theta_0)\sim 0.5$] (see also similar calculation in Ref. 30). Therefore, fitting the measured $T_T(\text{meas})$ with this new $T_T(\text{calc})$ would require less absorption or larger inverted $\omega_{368}$. The actual $\omega_{368}$ retrievals (Fig. 3) show that increase in input $n_{440}(=n_{368})$ does cause the increase in inverted $\omega_{368}$ in agreement with our estimate. Less pronounced jumps in $\omega_{368}$ retrievals caused by changes in AERONET input parameters can be seen on other retrieval days and times (Figs. 1 to 3). However, the jumps were typically within the range of overlap of $\omega$ retrieval uncertainty, and were considered insignificant.

Table 1 provides $\omega$ comparison statistics on days with high aerosol loadings [$\tau_{\text{ext}}(440)>0.4$], (60 matchups mostly in summer 2003), when both retrievals were most accurate. It was found that on average $\omega$ was lower at 368 nm ($\langle\omega_{368}\rangle=0.94$) than at 440 nm ($\langle\omega_{440}\rangle=0.96$). However, the mean $\omega$ differences (0.02) were within uncertainties of UV-MFRSR retrievals ($\sim$0.03, see the appendix). Note also that for AERONET wavelengths, $\omega$ increases with decreasing $\lambda$ in the visible for fine mode smoke or pollution aerosol.[27] Therefore, the extrapolated differences in $\omega_{368}$ (predicted by AERONET) and $\omega_{368}$ retrieved by UV-MFRSR may be slightly greater than direct compari-

**Table 1** Summer (2003) aerosol single scattering albedo statistics.[1]

| | | UV-MFRSR[2] | | | AERONET[3] | |
|---|---|---|---|---|---|---|
| Parameter | | 325 nm | 332 nm | 368 nm | 440 nm | 670 nm |
| Mean single scattering albedo, $\omega$ | $\langle\omega\rangle$ ($\omega_{min}$:$\omega_{max}$) | 0.92 (0.86:0.95) | 0.92 (0.86:0.95) | 0.94 (0.89:0.97) | 0.96 (0.91:0.99) | 0.95 (0.88:0.99) |
| Standard deviation, $\omega$ | $\sigma_\omega$ | 0.025 | 0.024 | 0.02 | 0.017 | 0.021 |
| Mean $\omega$ difference | $\langle\Delta\omega_\lambda\rangle=\langle\omega_{440}-\omega_\lambda\rangle$ | 0.04 (0.0:0.09) | 0.04 (0.0:0.09) | 0.02 (0.0:0.06) | 0 | 0.007 (0.0:0.03) |
| Standard deviation of $\Delta\omega_\lambda$ | $\sigma_{\Delta\omega\lambda}$ | 0.02 | 0.019 | 0.015 | 0 | 0.01 |
| Correlation coefficient $\omega_\lambda$ with $\omega_{440}$ | $R(\omega_\lambda,\omega_{440})$ | 0.61 | 0.61 | 0.67 | 1 | 0.95 |
| Correlation coefficient $\omega_\lambda$ with $\omega_{368}$ | $R(\omega_\lambda,\omega_{368})$ | 0.92 | 0.92 | 1 | 0.67 | 0.59 |

[1]Data sample ($N=60$) with solar zenith angle between 45 and 70 deg, $\tau_{440}>0.4$ was predominantly for summer 2003.

[2]Sample included 2-h-averaged UV-MFRSR $\omega$ retrievals (between 10 and 40 individual retrievals).

[3]Sample included individual AERONET $\omega$ inversions.

sons of $\omega_{440}$ to $\omega_{368}$. The inferred $\omega$ was even lower at shorter UV wavelengths ($\langle\omega_{325}\rangle$ to $\langle\omega_{332}\rangle=0.92$) that might suggest the presence of selectively UV absorbing aerosols or gases other than ozone.[55] The spectral differences between 325 and 332 nm were statistically insignificant, which could be explained by small separation in wavelength (7 nm) between these two channels. All $\omega$ spectral retrievals were highly correlated for either UV-MFRSR or AERONET inversions (correlation coefficient $>0.9$, Table 1). However, the correlation was weaker between UV-MFRSR and AERONET wavelengths.

The average AERONET $\omega$ retrievals for summer 2003 ($\langle\omega_{440}\rangle=0.96$) were lower than multiyear average at the same site[27] ($\langle\omega_{440}\rangle=0.98$), suggesting unusually high absorption. This difference could be a result of a statistical fluctuation (our sample includes only 60 cases, while much larger sample was used in Ref. 27) or could reflect real interannual changes in aerosol absorption. Since the $\omega$ retrievals were correlated in the UV and visible wavelengths (correlation coefficient $\sim$0.6 to 0.7) this could also mean that the true (multiyear) climatological absorption in UV wavelengths is, perhaps, higher by $\sim$0.02 than 2003 summer mean value ($\langle\omega_{368}\rangle=0.94$, Table 1). Continuation of the long-term continuous measurements by both techniques is therefore important to increase statistical significance of our results.

The results in Table 1 were obtained under conditions of high aerosol loadings [$\tau_{ext}(440)>0.4$] that were mostly restricted to summer humid haze conditions. The aerosol loadings are typically much lower at GSFC site in fall, winter, and spring seasons. The key question is whether the aerosol absorption remains seasonally independent and whether the $\omega$ results obtained during summer conditions (Table 1) could be used for other seasons. To investigate this question, the UV-MFRSR $\omega$ retrievals were repeated allowing cases with lower aerosol loadings [$\tau_{ext}(440)>0.1$] and correlated versus $\tau_{ext}$. The largest correlation between $\omega$ and $\tau_{ext}$ (with correlation coefficient $\sim$0.7) was found at 368 nm (Fig. 4), while correlation was weaker at other wavelengths ($\sim$0.6 at 325 nm and $\sim$0.4 at 440 and 670 nm). The decrease of $\omega$ with $\tau_{ext}$ suggests that the type of aerosol may have changed between summer and winter conditions. It is well known that aerosols in the mid-Atlantic region in summer are strongly hydroscopic,[52] therefore particle growth by swelling at a high relative humidity may be partly the reason for reduced absorption in summer.[27] Indeed, annual cycle of $\omega_{368}$ is the same as the $\tau_{ext}$ annual cycle: with maximum in summer and minimum in winter. A limited number of previous $\omega$ retrievals in the UV revealed larger variability of $\omega$ at different locations.[7,24,37–42] For example, $\omega$ retrievals using all channels of UV-MFRSR were conducted at Black Mountain, North Carolina.[38,40,41] The authors report $\omega_{368}$ ranging from 0.81 to 0.99 with the average value $\langle\omega_{368}\rangle=0.89$ and estimated uncertainty $\pm0.04$ at $\tau_{ext}\sim1$. On the other hand, estimates of $\omega_{325}$ in Toronto, Canada, using total (global) irradiance measured with a Brewer spectrophotometer ($\omega_{325}\sim0.95$ see Table 1 and Fig. 12 in Krotkov et al.[7]) were only insignificantly higher than current UV-MFRSR summer average value $\langle\omega_{368}\rangle=0.94$ at the GSFC location.

### 4.2 *Imaginary Part of Refractive Index*

Incorporating aerosol Mie calculations along with AERONET inversions of the particle size distributions and the real part of refractive index into the RT forward model made it possible to infer optically effective imaginary part of refractive index $k$ independently in each UV-MFRSR spectral channel (for details see Sec. 3). The combined statistics of UV-MFRSR and AERONET spectral $k$ retrievals on hazy summer days [$\tau_{ext}(440)>0.4$] is presented in Table 2. The retrieved $k$ values were higher in UV than in the visible wavelengths: $\langle k_{368}\rangle\sim0.009\pm0.004$ compared to $\langle k_{440}\rangle\sim0.006\pm0.003$. However, mean differences in $k$ ($\langle k_{368}-k_{440}\rangle\sim0.004,\sigma_{k_{368}-k_{440}}\sim0.003$) were only slightly larger than AERONET quoted[27] retrieval uncertainty $\Delta k\sim0.003$. The $k$ values were even higher at shorter UV wavelengths: $\langle k_{325}\rangle\sim0.013\pm0.005$. Therefore, the $k$ spectral dependence in the UV was found to be similar to the spectral absorption of organic carbon (OC) from biomass burning (Table 4 in Ref. 23), while AERONET $k$ retrievals were more consistent with the assumption that black carbon (BC, from urban and motor vehicle

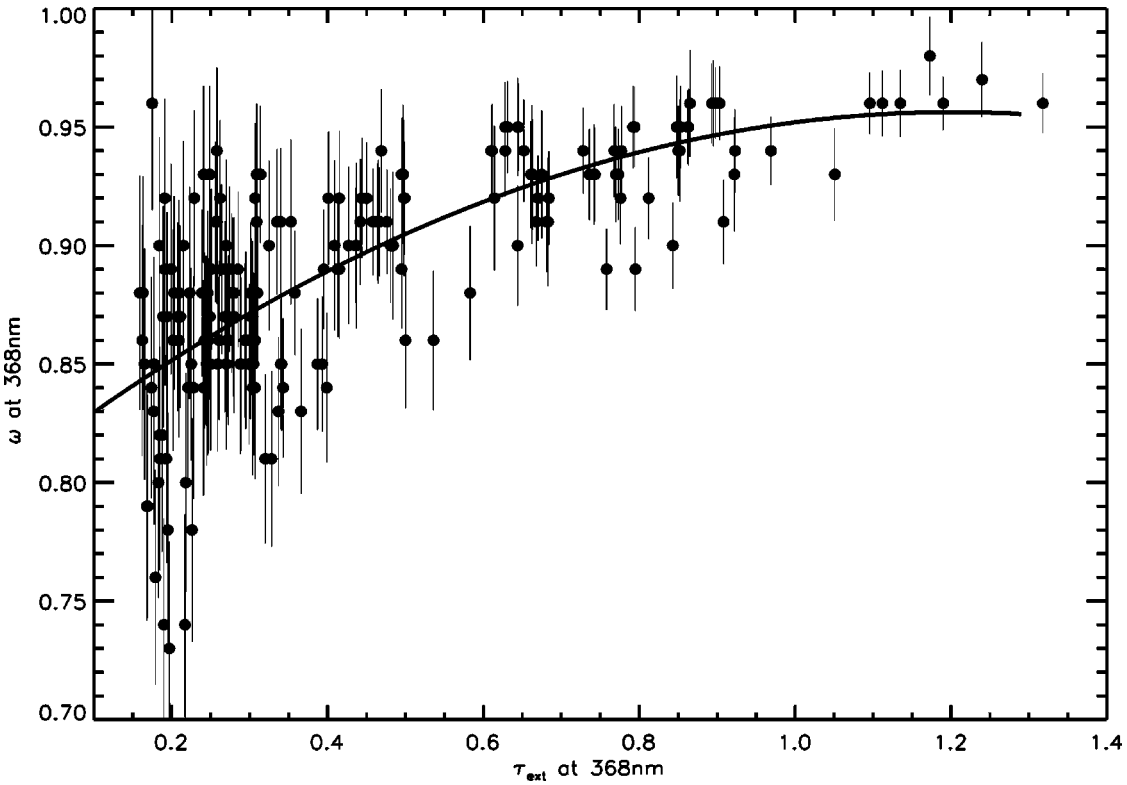


**Fig. 4** Hourly average retrieved values $\langle \omega_{368} \rangle$ as a function of measured extinction optical thickness $\tau_{abs}$ at 368 nm for 17 months of UV-MFRSR operation at NASA GSFC site in Maryland. The error bars are interpolated from Table 4 in the appendix and are the same as for individual retrievals. The error bars were not reduced, despite 1-h averaging of individual retrievals, because retrieval errors were not believed to be random. Only $\langle \omega_{368} \rangle$ values with estimated retrieval uncertainties less than 0.05 are shown.

emissions.[17–21] was the main absorber in the visible wavelengths.[27] These apparent differences require further investigation.

So far, UV-MFRSR $\omega$ and $k$ results (Tables 1 and 2) do not enable explanation of the causes of apparent larger absorption in the UV wavelengths compared to AERONET retrievals in the visible wavelengths. This could be due to differences in the techniques or the presence of selectively absorbing aerosols in the UV and requires further study. Enhancing both techniques to provide a spectral overlap with at least one common wavelength would provide better insight on aerosol absorption spectral dependence. At the same time, conducting colocated measurements at different sites with varying background aerosol conditions is also desirable.

### 4.3 *Aerosol Absorption Optical Thickness*

Ultimately, our goal with UV-MFRSR measurements was to derive the statistical distribution (daily and seasonal) of

**Table 2** Summer (2003) Imaginary refractive index statistics.[1]

| | | UV-MFRSR[2] | | | AERONET[3] | |
|---|---|---|---|---|---|---|
| Parameter | | 325 nm | 332 nm | 368 nm | 440 nm | 670 nm |
| Mean absorption index, $10^3 k$ | $10^3\langle k \rangle$<br>$10^3(k_{min}:k_{max})$ | 13<br>(7:27) | 13<br>(7:26) | 9<br>(5:20) | 6<br>(0.8:13) | 5<br>(0.8:12) |
| Standard deviation, $k$ | $10^3\sigma_k$ | 5 | 5 | 4 | 3 | 2.82 |
| Mean $k$ difference: $10^3\Delta k_\lambda$ | $10^3\langle k_\lambda - k_{440} \rangle$ | 7.6<br>(0:20) | 7<br>(0:19) | 3.6<br>(−1:12) | 0 | 0.3<br>(−1:1) |
| Standard deviation of the $k$ difference | $10^3\sigma_{\Delta k\lambda}$ | 3.7 | 3.6 | 2.5 | 0 | 0.4 |
| Correlation coefficient $k_\lambda$ with $k_{440}$ | $R(k_\lambda, k_{440})$ | 0.69 | 0.68 | 0.75 | 1 | 0.99 |
| Correlation coefficient $k_\lambda$ with $k_{368}$ | $R(k_\lambda, k_{368})$ | 0.95 | 0.95 | 1 | 0.75 | 0.73 |

[1]Sample ($N=60$) for solar zenith angle between 45 and 70 deg, and $\tau_{440}>0.4$ predominantly for summer 2003.

[2]Sample included 2-h-averaged UV-MFRSR $k$ retrievals (10 to 30 individual retrievals).

[3]Sample included individual AERONET $k$ inversions.

the UV absorption optical depth $\tau_{abs}$ at urbanized regions in the eastern part of the United States.[5] The $\tau_{abs}=\tau_{ext}(1-\omega)$ can be calculated using UV-MFRSR $\tau_{ext}$ and $\omega$ inversions or directly using linear regressions (see Fig. 7 in the appendix). Note that using regressions to estimate $\tau_{abs}$ directly from irradiance measurements enables retrievals under smaller aerosol loadings than possible with existing methods. An additional advantage is that $\tau_{ext}$ is typically 50 to 100% larger in the UV than in the visible wavelengths for urban-industrial aerosol with the same mass loading. These conditions make it possible to estimate $\tau_{abs}$ for smaller aerosol loadings [$\tau_{abs}(440)>0.1$], which in turn enabled, for the first time, studying the seasonal cycle in aerosol absorption. Figure 5 shows a time series of hourly $\langle\tau_{abs}(325)\rangle$ values for 17 months of continuous monitoring at GSFC site (cloud-free and snow-free cases). Also see Table 3.

The data gaps occurred due to unusually unfavorable weather conditions (rain or snow) in 2003 or from exceptionally clear days with $=\tau_{ext}(440)<0.1$. The main features of the $\tau_{abs}$ seasonal cycle at GSFC can be clearly seen from the figure: a pronounced summertime maximum with $\tau_{abs}(325)\sim0.08$ to 0.10 and wintertime minimum $\sim0.01$. The maximum $\tau_{abs}$ typically occurs in summer due to combination of regional and local pollution sources with hot and humid weather conditions (summer haze). The weakly absorbing haze is often associated with enhances high levels of tropospheric ozone[5] (ozone smog episodes). These summer haze conditions are responsible for summer high $\tau_{abs}$ values (at 368 nm $\sim0.06$ to 0.07). Even on relatively clear summer days, $\tau_{abs}$ is larger than $\sim0.02$. On top of the seasonal cycle, occasional transient phenomena (long-range transport of biomass burning smoke and desert dust storms) can be clearly detected. One clear example was the passage of an aged smoke plume from Siberian forest fires over GSFC on June 2, 2003 (Fig. 1), characterized by an unusually large $\tau_{abs}(325)\sim0.11$. Although occasional dust plumes had been reported at GSFC (for example, the April 2001 Asian dust plume), no dust events occurred during reported time period.

While the annual cycle in $\tau_{abs}$ is caused mainly by the annual cycle in aerosol extinction optical thickness $\tau_{ext}$, the correlation between $\tau_{abs}$ and $\tau_{ext}$ was not perfect (linear correlation coefficient $\sim0.76$ at 368 nm), as would have been the case with no variability in aerosol single scattering albedo, $\omega$=const. Indeed, $\omega_{368}$ data presented in Fig. 4 (as well as at other wavelengths) might suggest that $\omega$ is, indeed, not constant, but decreases with decreasing $\tau_{ext}$. The downward $\omega$ trend was seen for both UV-MFRSR and AERONET inversions, despite progressively larger retrieval errors at small $\tau_{ext}$. This trend could be due to real changes in the average aerosol composition between summer and winter months at the GSFC site.

## 5 Explaining Bias in Satellite UV Irradiance Retrievals

Aerosol UV absorption results reported here have important implications for measuring UV surface irradiance from space.[7,8] Multiyear comparisons of the TOMS UV data with ground-based Brewer measurements revealed a positive bias at many locations.[9–13] The bias can be seen at all wavelengths in clear-sky conditions. This suggests the difference is not related to ozone absorption. Here we estimate possible bias explanation due to aerosol absorption effects.[10,54] The TOMS UV algorithm first involves estimation of a clear-sky surface irradiance $E_{clear}$, which is adjusted to actual surface irradiance $E$ by using a TOMS-derived cloud/aerosol transmittance factor $C_T$:

$$E=E_{clear}C_T. \tag{2}$$

Either cloud or absorbing aerosol index (AI) correction is applied[7–10] to calculate $C_T$. Currently, absorbing aerosols are assumed and AI correction is applied if AI>0.5 and 360-nm reflectivity <0.15. Otherwise, cloud $C_T$ model is assumed, so the algorithm does not distinguish between

**Table 3** Annual (2002 to 2004) aerosol absorption optical thickness $\tau_{abs}$ statistics.[1]

| | | UV-MFRSR[2] | | | AERONET[3] | |
|---|---|---|---|---|---|---|
| Parameter | | 325 nm | 332 nm | 368 nm | 440 nm | 670 nm |
| Mean $\tau_{abs}$ | $\langle\tau_{abs}\rangle$ ($_{min}$:$_{max}$) | 0.05 (0.007:0.12) | 0.05 (0.009:0.11) | 0.04 (0.007:0.09) | 0.02 (0.003:0.05) | 0.01 (0.001:0.03) |
| Standard deviation, $\tau_{abs}$ | $\sigma_{\tau abs}$ | 0.02 | 0.02 | 0.015 | 0.01 | 0.007 |
| Mean $\tau_{abs}$ difference | $\Delta\tau_{abs}(\lambda)=\langle\tau_{abs}(\lambda)-\tau_{abs}(440)\rangle$ | 0.03 (−0.001:0.08) | 0.03 (−0.001:0.07) | 0.02 (−0.01:0.05) | 0 | −0.01 (−0.03:−0.002) |
| Standard deviation of the difference $\Delta\tau_{abs}(\lambda)$ | $\sigma_{\Delta\tau_{abs}}$ | 0.014 | 0.013 | 0.01 | 0 | 0.005 |
| Correlation coefficient $\tau_{abs}(\lambda)$ with $\tau_{abs}(440)$ | $R[\tau_{abs}(440),\tau_{abs}(\lambda)]$ | 0.84 | 0.81 | 0.76 | 1 | 0.98 |
| Correlation coefficient $\tau_{abs}(\lambda)$ with $\tau_{abs}(368)$ | $R[\tau_{abs}(368),\tau_{abs}(\lambda)]$ | 0.93 | 0.95 | 1 | 0.76 | 0.74 |

[1]Data sample ($N=260$) with solar zenith angle between 20 and 70 deg, and $\tau_{440}>0.1$ in 2002 to 2004.

[2]Sample included 2-h-averaged UV-MFRSR *k* retrievals (between 10 and 40 individual retrievals).

[3]Sample included individual AERONET *k* inversions.

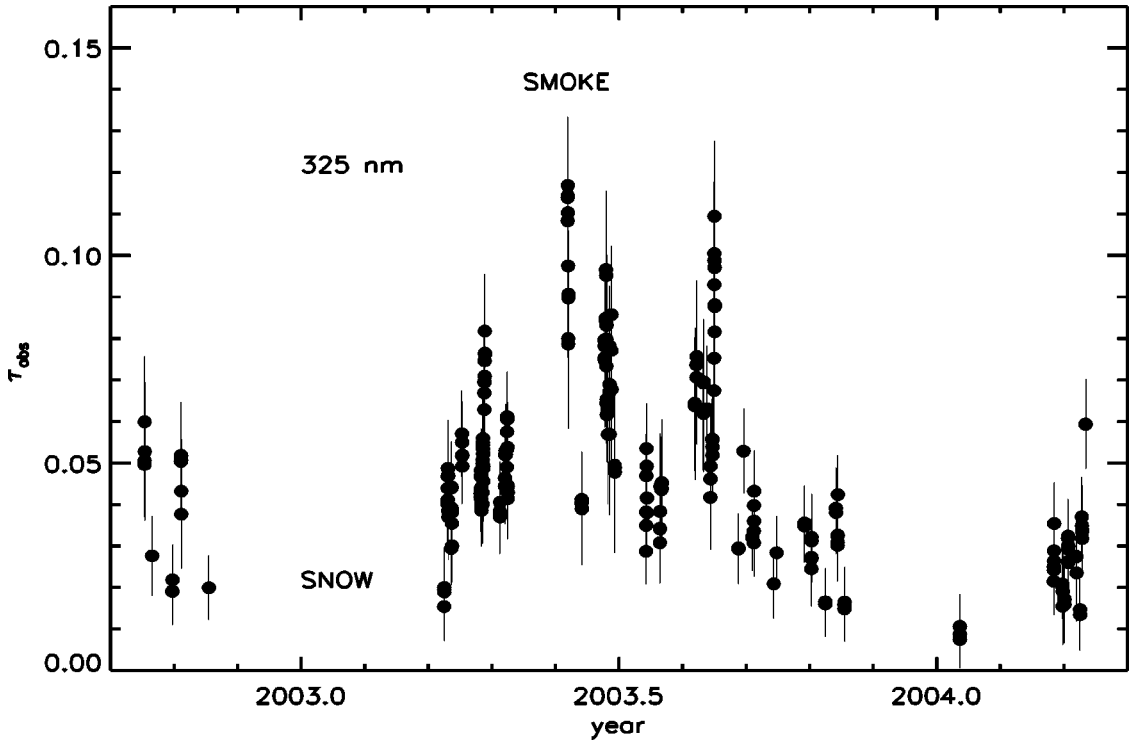


**Fig. 5** Time series of aerosol absorption optical thickness $\tau_{abs}$ at 325 nm derived from 17 months of UV-MFRSR operation at NASA GSFC site in Maryland. The data are for cloud-free and snow-free conditions. Individual $\tau_{abs}$ values were averaged over a 2-h period of time within $\pm 60$ min of the AERONET inversion. The error bars of $\tau_{abs}$ are interpolated from estimates given in the appendix in Table 4.

thin clouds and aerosols. This causes a typical $C_T$ error $\sim 2\%$ for nonabsorbing sulfate or sea salt aerosols with $\tau_{ext}(550) = 0.2$. On the other hand, absorbing aerosols in the boundary layer attenuate UV irradiance more strongly for the same $\tau_{ext}$ (see Appendix), causing cloud $C_T$ correction to underestimate their attenuation of surface UV irradiance. Because pollution aerosols are typically located in the boundary layer, they tend to produce negative AI, which makes it impossible to distinguish from nonabsorbing aerosols and thin clouds using just AI data, causing overestimation of UV irradiance. Moreover, since these aerosols also attenuate the outgoing radiation, the cloud $C_T$ algorithm underestimates $\tau_{ext}$, amplifying the error further. The TOMS UV bias was modeled and shown[10,54] to be proportional to $\tau_{abs}$. Here we quantified the bias using actual TOMS and UV-MFRSR measurements combined with retrievals of the aerosol optical properties as follows:

1. Atmospheric radiances were measured by TOMS at 331 and 360 nm and inverted with a standard TOMS surface UV algorithm[10] to obtain estimates of surface UV irradiance at 325 nm, UV(TOMS).
2. The TOMS absorbing AI was also calculated to select conditions with no free-troposphere absorbing aerosol plumes: AI$<0.5$.
3. UV(TOMS) was compared with the UV-MFRSR measured total UV irradiance to estimate the bias: UV(TOMS)/UV(ground).
4. The bias was correlated with UV-MFRSR measurements of $\tau_{abs}(325\,\text{nm})$ (Fig. 6).

Figure 6 shows that the bias was indeed well correlated with $\tau_{abs}(325\,\text{nm})$ and the slope of the regression was close to the theoretically predicted parameterization. This confirms that boundary layer aerosol absorption can explain the positive TOMS UV bias found in ground-based land comparisons. Since operational global satellite UV algorithm was not expected to catch all variability in local atmospheric and geographical conditions at measurement sites, the bias was parameterized as function of $\tau_{abs}$ to provide off-line correction for the operational UV(TOMS) data, so users at sites with $\tau_{abs}$ ground measurements or established climatology can apply their own corrections to the standard TOMS UV data off-line.

$$\text{UV(corrected)} = \frac{\text{UV(TOMS)}}{1 + 3\,\tau_{abs}(\lambda)}. \tag{3}$$

## 6 Conclusions

First, it was demonstrated that an advantage of the shadowband technique in measuring aerosol absorption is that the accurate irradiance calibration can be established by calibrating the direct sun component and comparing with sunphotometers such as AERONET CIMELs. The shadowband method is complementary to the AERONET almucantar retrieval of aerosol single scattering albedo,[25–27] because the

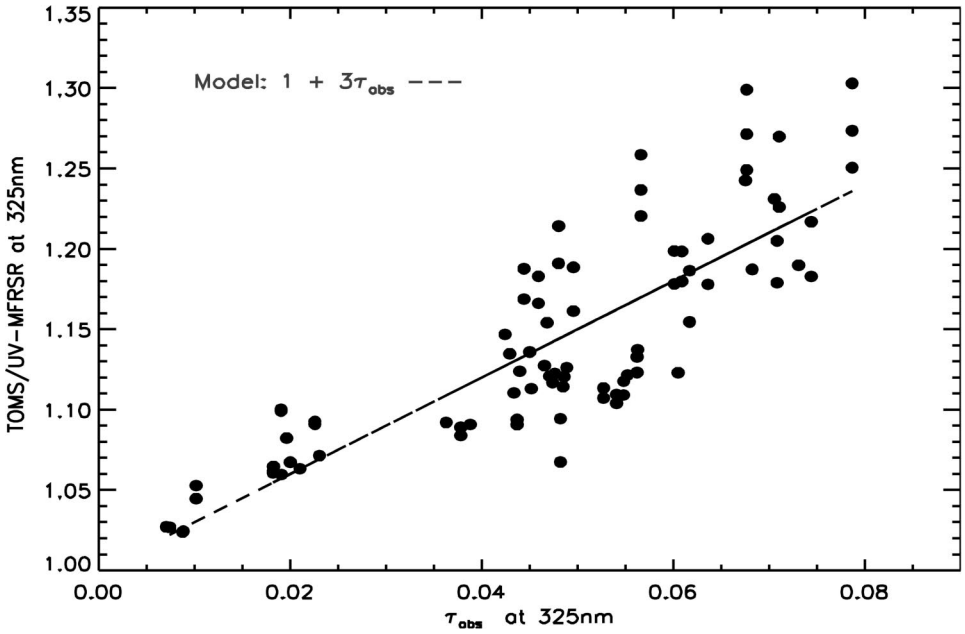


**Fig. 6** Ratio between satellite-estimated (by the TOMS UV algorithm[7–10]) and measured (by the UV-MFRSR) total (direct plus diffuse) surface UV irradiance at 325 nm versus aerosol absorption optical thickness at 325 nm inferred from combined UV-MFRSR and AERONET measurements at NASA GSFC site. The line shows a theoretical relationship derived from radiative transfer modeling.[10] The results are shown for only pollution aerosols with the TOMS absorbing AI at 331 nm less than 0.5 and TOMS 360-nm Lambertian effective reflectivity less than 0.15.

retrievals are more reliable at low solar zenith angles. Therefore, combined use of both instruments enables us to derive the complete diurnal cycle of aerosol absorption.

Second, there are specific advantages in measuring aerosol absorption in UV that lead us to believe that $\omega$ retrieval results can be used down to $\tau_{ext} \sim 0.2$: (1) the measured accuracy of AERONET reference instruments in the UV with additional pressure and true ozone corrections could be made better than the previously estimated value of $\sim 0.01$ at 340 nm;[35,36,47] (2) the surface albedo is much smaller in the UV than in the visible spectral region and does not affect the aerosol retrievals as much; (3) $\tau_{ext}$ in UV is larger (for the same aerosol mass) than in the visible spectral range; (4) careful characterization of the UV-MFRSR instrument, correction for known systematic errors, monitoring of instrument performance via daily CIMEL intercomparisons, and characterizing atmospheric conditions; (5) stability and repeatability of individual $\omega$ retrievals; and (6) ancillary and redundant aerosol measurements available at GSFC site. Indeed, measurement redundancy and instrument intercomparisons were key factors in helping to increase the accuracy of aerosol absorption measurements.

Third, inferred values of the effective UV imaginary refractive index were first used for comparisons of aerosol single scattering albedo $\omega$ at 325, 332, and 368 nm and with AERONET retrievals[25] at 440 nm, $\omega_{440}$. The measured differences in absorption between 368 and 440 nm might suggest the presence of selectively UV absorbing aerosols[22,23] or interference from gases other than ozone. However, the differences might also be caused by uncorrected systematic instrumental effects or absolute calibration uncertainties of sky radiances ($\sim$5% for almucantar technique[26]). Continuing colocated measurements at the GFSC location is important to improve the comparison statistics, but conducting these measurements at different sites with varying background aerosol conditions is also desirable.

Fourth, using all cases for cloud-free days, we derived the diurnal and seasonal dependence of aerosol absorption optical thickness $\tau_{abs}$ in the UV wavelengths. The expected accuracy of $\tau_{abs}$ retrieval from UV-MFRSR measurements is $\sim 0.01$ to 0.02, limited by the UV-MFRSR measured accuracy and calibration ($V_0$). The variability in aerosol size distribution and real refractive index becomes comparable to the measured uncertainties only for large aerosol loadings ($\tau_{ext} > 0.5$). The $\tau_{abs}$ values show a pronounced seasonal dependence of $\tau_{ext}$ with maximum values $\tau_{abs} \sim 0.1$ occurring in summer hazy conditions[5] and $<0.02$ in winter and fall seasons, when aerosol loadings are small.

Finally, it was found that $\omega$ decreases with decreases in $\tau_{ext}$. This could be due to real changes in the average aerosol composition between summer and winter months at the GSFC site. Obviously, continuation of UV-MFRSR measurements at the GSFC site with an enhanced unit (adding 440-nm channel) is important to increase confidence in reported data.

In the future we suggest

1. Providing spectral overlap measurements for shadowband and almucantar techniques. This involves absolute calibration of UV sky radiance channels of CIMEL instruments (340 and 380 nm) and extending almucantar inversion technique[25–27] to include UV sky scans. For the shadowband technique, replacing

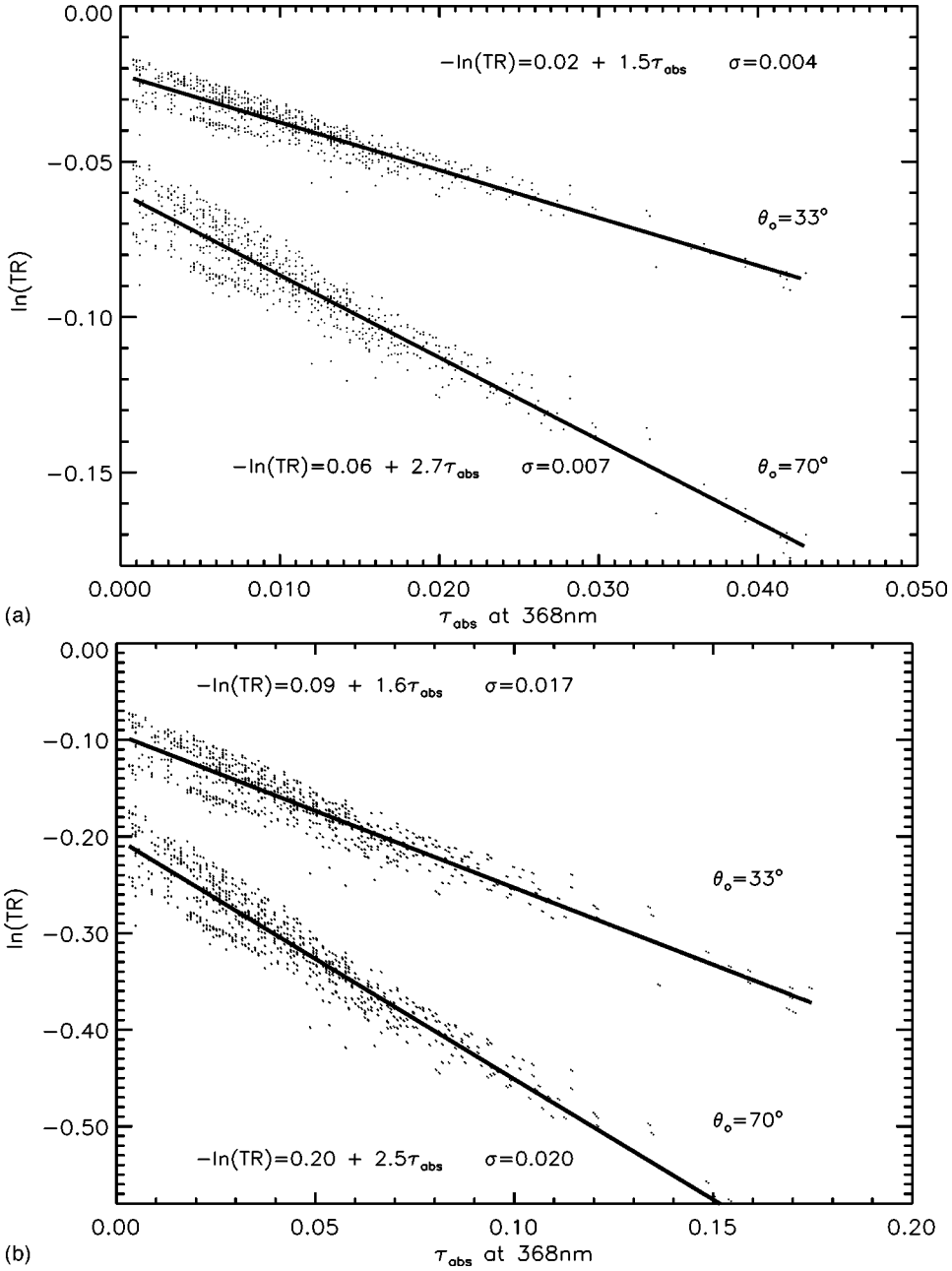


**Fig. 7** Relationship between Rayleigh normalized total transmittance, TR, and $\tau_{abs}$ at 368 nm, assuming fixed solar zenith angle (SZA) $\theta_0=33$ and 70 deg and extinction optical thickness (a) $\tau_{ext}=0.2$ (top) and (b) $\tau_{ext}=0.8$ (bottom). Linear regression model of Eq. (4) is fitted to all data points assuming variability due to size distribution as a random error. Regression coefficients are given in Table 4.

filters in one or several channels of the UV-MFRSR instrument to match those of CIMEL instrument will be also helpful.

2. Adding spectrometer measurements to separate between aerosol and gaseous absorption.[55]
3. Conducting measurements at different sites with larger expected UV aerosol absorption (more polluted sites with a higher BC fraction) or different types of aerosol (for sites with predominantly dust larger absorption is expected in UV than in the visible).

## 7 Appendix: Sensitivity of UV-MFRSR Measurements to Aerosol Absorption

Standard UV-MFRSR measurements include voltages that are proportional to total horizontal and diffuse horizontal irradiance components. Since both components are measured by the same diffuser/filter/detector combination, diffuse and total atmospheric transmittances are obtained directly from the measured voltage ratios: $T_D=V_D/V_0$ and $T_T=V_T/V_0$. Here $V_0$ is extraterrestrial voltage obtained by calibration transfer from AERONET network sunphotometers[35,36] as previously described.[45] The diffuse

**Table 4** UV-MFRSR measurement errors, sensitivity to $\tau_{abs}$ for different conditions and expected retrieval errors.

| Sources of measured errors in UV-MFRSR 368-nm channel | $\tau_{ext}=0.2$ | | $\tau_{ext}=0.8$ | |
|---|---|---|---|---|
| | $\theta_0=33$ | $\theta_0=70$ | $\theta_0=33$ | $\theta_0=70$ |
| | Daily $V_0$ calibration error, $\sigma_{\ln V_0}$ | | | |
| $\Delta \ln V_0$ (V0~2100 mv)[1] | | | | |
| $\sigma_{\ln V_0}$ | 0.01(0.05) | 0.01(0.05) | 0.02(0.1) | 0.02(0.1) |
| | Combined TR measurement and calibration errors | | | |
| Combined TR measurement error[2] | | | | |
| $\sigma_{\ln(TR)}$ | ~0.022(0.05) | ~0.022(0.05) | ~0.036(0.1) | ~0.036(0.1) |
| | Measurement sensitivity: $\frac{\partial \ln(V_T)}{\partial(\tau_y)}$ | | | |
| Sensitivity $\ln(V_T/V_0)$ to $\tau_{abs}$ | 1.5 | 2.7 | 1.6 | 2.5 |
| Sensitivity $\ln(V_T/V_0)$ to $\tau_{ext}$ | 0.1 | 0.17 | 0.1 | 0.17 |
| | Expected retrieval errors | | | |
| Expected error in $\tau_{abs}$ due to measurement error, $1\sigma$ | 0.01(0.03) | 0.008(0.02) | 0.02(0.05) | 0.014(0.05) |
| Expected error[3] in $\tau_{abs}$ due to uncertainty in PSD, $1\sigma$ | 0.006 | 0.003 | 0.01 | 0.01 |
| Combined error in $\tau_{abs}$, $1\sigma$ | 0.012(0.03) | 0.008(0.02) | 0.022(0.051) | 0.017(0.05) |
| Error[4] in $\omega \sim \frac{\Delta \tau_{abs}}{\tau_{ext}}$ | 0.06(0.15) | 0.04(0.10) | 0.03(0.06) | 0.02(0.06) |

[1]AERONET $V_0$ uncertainty for reference instruments combined with calibration transfer error (see Part 1 paper).[45]

[2]Assuming that calibration and $V_T$ measurement errors are uncorrelated (see part 1 paper).[45]

[3]The scatter of points around regression line [Eq. (4) in appendix] gives estimate of the retrieval noise if size distribution information is not used in $\tau_{abs}$ retrieval (Fig. 7).

[4]Using relationship $\omega=1-\tau_{abs}/\tau_{ext}$, assuming constant error in $\tau_{ext}$: $\sigma_{\tau_{ext}}\sim 0.01$ and uncorrelated errors in errors in $\tau_{ext}$ and $\tau_{abs}$. Numbers in parentheses refer to on-site Langley calibrations.

and total transmittances are not independent, since the voltage difference $(V_T-V_D)$ has been used for the direct-sun equivalent calibration $V_0$ and to infer aerosol extinction optical thickness $\tau_{ext}$. Therefore, only one additional aerosol parameter could be independently estimated in each UV-MFRSR spectral channel by matching transmittances for each wavelength (or their ratios) to those calculated from a radiative transfer model. Our goal is to infer aerosol absorption optical thickness $\tau_{abs}$ while other model input parameters are constrained by independent measurements. Note that the UV surface albedo is low and stable at our site for snow-free conditions (~0.02 to 0.03 from clear-sky overpass EP-TOMS reflectivity measurements) and does not have a noticeable effect on ground-based aerosol measurements.

Historically, different irradiance ratios were used to infer $\tau_{abs}$ (or aerosol single scattering albedo, $\omega=1-\tau_{abs}/\tau_{ext}$): diffuse/direct ratio,[29–31] $DD=T_D/(T_T-T_D)$, diffuse fraction (diffuse/total, $DT=T_D/T_T$) ratio,[32–34] and total to Rayleigh transmittance ratio[7] $(TR=T_T/T_{Ray})$. In the end, all inversion techniques should deliver consistent $\tau_{abs}$ retrieval results regardless of which ratios are used. For our measurements of $\tau_{abs}$, the most convenient quantity is the total $(T_T=\text{direct plus diffuse})$ atmospheric transmittance, which is directly related to aerosol absorption and is least sensitive to aerosol size distribution and extinction optical thickness $\tau_{ext}$. In the UV spectral region, where $\tau_{Rayleigh}$ typically exceeds that of $\tau_{aerosol}$, it is convenient to normalize $T_T$ by the total transmittance of the molecular atmosphere with the same ozone amount, $TR=T_T/T_{Ray}$, which greatly reduces sensitivity to ozone, wavelength, and solar zenith angle. An important advantage of working with TR is that nonabsorbing aerosols have only a small effect[7] on TR ($\tau\sim 0.1$ produces ~1% TR reduction), since the decrease in direct solar flux caused by aerosol scattering is nearly compensated by an increase in diffuse sky flux. For UV absorbing aerosols (dust, smoke, and urban), the increase in the diffuse flux is suppressed by aerosol absorption, so TR sensitivity to $\tau_{abs}$ is an order of magnitude greater than TR sensitivity to $\tau_{ext}$. Based on a modeling study,[7] the dependence of TR on $\tau_{ext}$ and $\tau_{abs}$ can be written approximately as

$$-\ln(\mathrm{TR}) \approx a\,\tau_{ext} + b\,\tau_{abs}, \tag{4}$$

where, for typical aerosols (not containing significant quantities of mineral dust and smoke), $a\sim 0.1$ and $b\sim 2-3$ (increasing with solar zenith angle). To better estimate $a$ and

$b$, TR and $\tau_{abs}$ were recalculated for fixed values of solar zenith angle $\theta_0$ and $\tau_{ext}$ using AERONET individual almucantar inversions[25–27] at GSFC in 2002 to 2003.

The linear regression model [Eq. (4)] was fitted to all calculated pairs $(T_R, \tau_{abs})$ to estimate $T_R$ sensitivity selectively to $\tau_{abs}$, treating real variability in size distribution and real part of refractive index $n_R$ as random errors (Fig. 7).

The regression coefficients quantify TR sensitivity to aerosol parameters as function of SZA (Table 4). The expected accuracy of $\tau_{abs}$ retrieval from UV-MFRSR measurements is ~0.008 to 0.02, limited by the measured accuracy of total voltage ($V_T$) and calibration[45] ($V_0$). The variability in aerosol size distribution and real refractive index becomes comparable to the measured uncertainties only for large aerosol loadings ($\tau_{ext} > 0.5$). The measurement uncertainties (discussed in detail in the first paper[45]) and regression coefficients for high and low aerosol loadings are summarized in Table 4. The estimated retrieval uncertainties of $\tau_{abs}$ and $\omega$ for the shadowband technique (Table 4) are comparable to the almucantar technique[25–27] for favorable conditions [large SZAs, $\theta_0 > 45$ deg and high aerosol loadings $\tau_{ext}(440\,\text{nm}) > 0.4$]. However, an important advantage of the shadowband technique is that it remains sensitive to $\tau_{abs}$ even at low solar zenith angles, when the almucantar technique is not sensitive[25–27] to $\tau_{abs}$. On the other hand, cosine-correction errors increase for shadowband measurements at high SZAs (see discussion in Ref. 45), while cosine errors are absent for the CIMEL. Thus, the two types of measurements are required for measuring complete diurnal cycle of aerosol absorption.

## Acknowledgments

We thank members of USDA UVMRP and NASA AERONET projects for their support. We acknowledge NASA's Office of Earth Science (Code YS) for continued support through the TOMS Science Team and thank an anonymous reviewer for suggesting substantial improvements to the paper.

## References

1. R. V. Martin, D. J. Jacob, R. N. Yantosca, M. Chin, and P. Ginoux, "Global and regional decreases in tropospheric oxidants from photochemical effects of aerosols," *J. Geophys. Res.* **108**(D3), 4097 (2003); (doi:10.1029/2002JD002622).
2. S. He and G. R. Carmichael, "Sensitivity of photolysis rates and ozone production in the troposphere to aerosol properties," *J. Geophys. Res.* **104**, 26307–26324 (1999).
3. H. Liao, Y. L. Yung, and J. H. Seinfeld, "Effects of aerosols on tropospheric photolysis rates in clear and cloudy atmospheres," *J. Geophys. Res.* **104**, 23697–23707 (1999).
4. M. Z. Jacobson, "Studying the effects of aerosols on vertical photolysis rate coefficient and temperature profiles over an urban airshed," *J. Geophys. Res.* **103**, 10593–10604 (1998).
5. R. R. Dickerson, S. Kondragunta, G. Stenchikov, K. L. Civerolo, B. G. Doddridge, and B. N. Holben, "The impact of aerosols on solar ultraviolet radiation and photochemical smog," *Science* **28**, 827–830 (1997).
6. S. Madronich, "UV radiation in the natural and perturbed atmosphere," in *Environmental Effects of Ultraviolet (UV) Radiation*, pp. 17–69, Lewis Publisher, Boca Raton, FL (1993).
7. N. A. Krotkov, P. K. Bhartia, J. R. Herman, V. Fioletov, and J. Kerr, "Satellite estimation of spectral surface UV irradiance in the presence of tropospheric aerosols 1. Cloud-free case," *J. Geophys. Res.* **103**(D8), 8779–8793 (1998).
8. J. R. Herman, N. Krotkov, E. Celarier, D. Larko, and G. Labow, "The distribution of UV radiation at the earth's surface from TOMS measured UV-backscattered radiances," *J. Geophys. Res.* **104**, 12059–12076 (1999).
9. N. A. Krotkov, J. R. Herman, P. K. Bhartia, C. Seftor, A. Arola, J. Kurola, S. Kalliscota, P. Taalas, and I. Geogdzhaev, "Version 2 TOMS UV algorithm: problems and enhancements," *Opt. Eng.* **41**(12), 3028–3039 (2002).
10. N. A. Krotkov, J. R. Herman, P. K. Bhartia, C. Seftor, A. Arola, J. Kaurola, P. Taalas, I. Geogdzhaev, and A. Vasilkov, *OMI Surface UV Irradiance Algorithm*, P. Stammes, Ed., Vol. 3, ATBD-OMI_03 (http://eospso.gsfc.nasa.gov/eos_homepage/for_scientists/atbd/docs/OMI/ATBD-OMI-03.pdf).
11. V. E. Fioletov, J. B. Kerr, D. I. Wardle, N. Krotkov, and J. R. Herman, "Comparison of Brewer ultraviolet irradiance measurements with total ozone mapping spectrometer satellite retrievals," *Opt. Eng.* **41**(12), 3051–3061 (2002).
12. J. B. Kerr, G. Seckmeyer, A. F. Bais, G. Bernhard, M. Blumthaler, S. B. Diaz, N. Krotkov, D. Lubin, R. L. McKenzie, A. A. Sabziparvar, and J. Verdebout, "Surface ultraviolet radiation: past and future," Chap. 5 in *Scientific Assessment of Ozone Depletion: 2002*, Global Ozone Research and Monitoring Project, Report N 47, World Meteorological Organization, Geneva (2003).
13. V. E. Fioletov, M. G. Kimlin, N. A. Krotkov, L. J. B. McArthur, J. B. Kerr, D. I. Wardle, J. R. Herman, R. Metltzer, T. W. Mathews, and J. Kaurola, "UV index climatology over North America from ground-based and satellite estimates," *J. Geophys. Res.* **109**(D2), 2308 (2004); (doi:10.1029/2004JD004820).
14. G. A. d'Almeida, P. Koepke, and E. P. Shettle, *Atmospheric Aerosols: Global Climatology and Radiative Characteristics*, A. Deepak Publ., Hampton, VT (1991).
15. I. N. Sokolik and O. B. Toon, "Incorporation of mineralogical composition into models of the radiative properties of mineral aerosol from UV to IR wavelengths," *J. Geophys. Res.* **104**(D8), 9423–9444 (1999).
16. S. C. Alfaro, S. Lafton, J. L. Rajot, P. Formenti, A. Gaudichet, and M. Maille, "Iron oxides and light absorption by pure desert dust: an experimental study," *J. Geophys. Res.* **109**(D0), 8208 (2004); (doi:10.1029/2003JD004374).
17. J. T. Twitty and J. A. Weinman, "Radiative properties of carbonaceous aerosols," *J. Appl. Meteorol.* **10**, 725–731 (1975).
18. H. Horvath, "Atmospheric light absorption—a review," *Atmos. Environ.* **27A**, 293–317 (1993).
19. J. D. Lindberg, R. E. Douglass, and D. M. Garvey, "Carbon and the optical properties of atmospheric dust," *Appl. Opt.* **32**(30), 6077–6081 (1993).
20. R. W. Bergstrom, P. B. Russell, and P. Hignett, "Wavelength dependence of the absorption of black carbon particles: predictions and results from the TARFOX experiment and implications for the aerosol single scattering albedo," *J. Atmos. Sci.* **59**, 567–577 (2002).
21. R. W. Bergstrom, P. Pilewskie, B. Schmid, and P. B. Russel, "Estimates of the spectral aerosol single scattering albedo and aerosol radiative effects during SAFARI 2000," *J. Geophys. Res.* **108**(D13), 8474 (2003); (doi:10.1029/2002JD002435).
22. M. Z. Jacobson, "Isolating nitrated and aromatic aerosols and nitrated aromatic gases as sources of ultraviolet light absorption," *J. Geophys. Res.* **104**, 3527–3542 (1999).
23. T. W. Kirchstetter, T. Novakov, and P. Hobbs, "Evidence that the spectral dependence of light absorption by aerosols is affected by organic carbon," *J. Geophys. Res.* **109**(D2), 1208 (2004); (doi:10.1029/2004JD004999).
24. R. W. Bergstrom et al., "Spectral absorption of solar radiation by aerosols during ACE-Asia," *J. Geophys. Res.* **198**(D19S15), 8474 (2004); (doi:10.1029/2003JD004467).
25. O. Dubovik and M. D. King, "A flexible inversion algorithm for retrieval of aerosol optical properties from sun and sky radiance measurements," *J. Geophys. Res.* **105**(D16), 20673–20696 (2000).
26. O. Dubovik, A. Smirnov, B. N. Holben, M. D. King, Y. J. Kaufman, T. F. Eck, and I. Slutsker, "Accuracy assessments of aerosol optical properties retrieved from Aerosol Robotic Network (AERONET) sun and sky radiance measurements," *J. Geophys. Res.* **105**(D8), 9791–9806 (2000).
27. O. Dubovik, B. Holben, T. Eck, A. Smirnov, Y. J. Kaufman, M. D. King, D. Tanre, and I. Slutsker, "Variability of absorption and optical properties of key aerosol types observed in worldwide locations," *J. Atmos. Sci.* **59**, 590–608 (2002).
28. T. F. Eck, B. N. Holben, J. R. Reid et al., "High aerosol optical depth biomass burning events: A comparison of optical properties for different source regions," *Geophys. Res. Lett.* **30**(20), 2035 (2003); (doi:10.1029/2003GL017861).
29. B. M. Herman, S. R. Browning, and J. J. DeLuisi, "Determination of the effective imaginary term of the complex refractive index of atmospheric dust by remote sensing: the diffuse-direct radiation method," *J. Atmos. Sci.* **32**, 918–925 (1975).
30. M. King and B. M. Herman, "Determination of the ground albedo and the index of absorption of atmospheric particles by remote sensing.

Part I: Theory,'' *J. Atmos. Sci.* **36**, 163–173 (1979).
31. M. King, ''Determination of the ground albedo and the index of absorption of atmospheric particles by remote sensing. Part II: Application,'' *J. Atmos. Sci.* **36**, 1072–1083 (1979).
32. T. F. Eck, B. N. Holben, I. Slutsker, and A. Setzer, ''Measurements of irradiance attenuation and estimation of aerosol single scattering albedo for biomass burning aerosols in Amazonia,'' *J. Geophys. Res.* **103**, 31865–31878 (1998).
33. T. F. Eck, B. N. Holben, D. E. Ward, M. M. Mukelabai, O. Dubovik, A. Smirnov, J. S. Schafer, N. C. Hsu, S. J. Piketh, A. Queface, J. Le Roux, R. J. Swap, and I. Slutsker, ''Variability of biomass burning aerosol optical characteristics in southern Africa during the SAFARI 2000 dry season campaign and a comparison of single scattering albedo estimates from radiometric measurements,'' *J. Geophys. Res.* **108**(D13), 8477 (2003); (doi:10.1029/2002JD002321).
34. T. A. Tarasova, I. A. Gorchakova, M. A. Sviridenkov, P. P. Anikin, and E. V. Romashova, ''Estimation of the radiative forcing of smoke aerosol from radiation measurements at the Zvenigorod scientific station in the summer of 2002,'' *Atmos. Oceanic Phys.* **40**(4), 454–463 (2004).
35. B. N. Holben et al., ''AERONET—a federated instrument network and data archive for aerosol characterization,'' *Remote Sens. Environ.* **66**, 1–16 (1998).
36. B. N. Holben et al., ''An emerging ground-based aerosol climatology: aerosol optical depth from AERONET,'' *J. Geophys. Res.* **106**, 12067–12097 (2001).
37. A. Kylling, A. F. Bais, M. Blumthaler, J. Schreder, C. S. Zerefos, and E. Kosmidis, ''Effect of aerosols on solar UV irradiances during the photochemical activity and solar ultraviolet radiation campaign,'' *J. Geophys. Res.* **103**, 26051–26060 (1998).
38. B. N. Wenny, J. S. Schafer, J. J. DeLuisi, V. K. Saxena, W. F. Barnard, I. V. Petropavlovskikh, and A. J. Vergamini, ''A study of regional aerosol radiative properties and effects on ultraviolet-B radiation,'' *J. Geophys. Res.* **103**(D14), 17083–17097 (1998).
39. J. Reuder and H. Schwander, ''Aerosol effects on UV radiation in nonurban regions,'' *J. Geophys. Res.* **104**, 4065–4077 (1999).
40. B. N. Wenny, V. K. Saxena, and J. E. Frederick, ''Aerosol optical depth measurements and their impact on surface levels of ultraviolet-B radiation,'' *J. Geophys. Res.* **106**, 17311–17319 (2001).
41. J. L. Petters, V. K. Saxena, J. R. Slusser, B. N. Wenny, and S. Madronich, ''Aerosol single scattering albedo retrieved from measurements of surface UV irradiance and a radiative transfer model,'' *J. Geophys. Res.* **108**(D9), 4288 (2003); (doi:10.1029/2002JD002360).
42. M. A. Wetzel, G. E. Shaw, J. R. Slusser, R. D. Borys, and C. F. Cahill, ''Physical, chemical, and ultraviolet radiative characteristics of aerosol in central Alaska,'' *J. Geophys. Res.* **108**(D14), 4418 (2003); (doi:10.1029/2002JD003208).
43. L. Harrison, J. Michalsky, and J. Berndt, ''Automated multi-filter rotating shadowband radiometer: an instrument for optical depth and radiation measurements,'' *Appl. Opt.* **33**, 5118–5125 (1994).
44. L. Harrison and J. Michalsky, ''Objective algorithms for the retrieval of optical depths from ground-based measurements,'' *Appl. Opt.* **33**, 5126–5132 (1994).
45. N. A. Krotkov, P. K. Bhartia, J. R. Herman, J. Slusser, G. Scott, G. Jason, G. Labow, T. F. Eck, and B. N. Holben, ''Aerosol ultraviolet absorption experiment (2002 to 2004): 1. ultraviolet multifilter rotating shadowband radiometers calibration and intercomparison with CIMEL sunphotometers,'' *Opt. Eng.* **44**, 041004 (2005).
46. D. S. Bigelov, J. R. Slusser, A. F. Beaubien, and J. R. Gibson, ''The USDA ultraviolet radiation monitoring program,'' *Bull. Am. Meteorol. Soc.* **79**, 601–615 (1998).
47. T. F. Eck, B. N. Holben, J. S. Reid, O. Dubovik, A. Smirnov, N. T. O'Neill, I. Slutsker, and S. Kinne, ''Wavelength dependence of the optical depth of biomass burning, urban and desert dust aerosols,'' *J. Geophys. Res.* **104**, 31333–31350 (1999).
48. J. R. Slusser, J. H. Gibson, D. Kolinski, P. Disterhoft, K. Lantz, and A. F. Beabien, ''Langley method of calibrating UV filter radiometer,'' *J. Geophys. Res.* **105**, 4841–4849 (2000).
49. J. R. Herman and E. Celarier, ''Earth surface reflectivity climatology at 340 to 380 nm from TOMS data,'' *J. Geophys. Res.* **102**, 28003–28011 (1997).
50. B. M. Herman, T. R. Caudill, D. E. Flittner, K. J. Thome, and A. Ben-David, ''A comparison of the Gauss-Seidel spherical polarized radiative transfer code with other radiative transfer codes,'' *Appl. Opt.* **34**, 4563–4572 (1995).
51. K. Stamnes et al., ''Numerically stable algorithm for descrete-ordinate-method radiative transfer in multiple scattering and emitting layered media,'' *Appl. Opt.* **27**, 2502–2509 (1988).
52. R. Kotchenruther and P. V. Hobbs, ''Humidification factors of aerosols from biomass burning in Brazil,'' *J. Geophys. Res.* **103**, 32081–32090 (1998).
53. J. A. Coakley, Jr. and P. Chylek, ''The two-stream approximation in radiative transfer: including the angle of the incident radiation,'' *J. Atmos. Sci.* **32**, 409–418 (1975).
54. Arola et al., ''Assessment of TOMS UV bias due to absorbing aerosols,'' in *UV Ground and Space-Based Measurements, Models and Effects IV*, J. R. Slusser, J. R. Herman, and G. G. Bernhard, Eds., *Proc. SPIE* **5545**, 28–35 (2004).
55. A. N. Bublev, N. E. Chubarova, A. N. Trotsenko, and G. I. Gorchakov, ''Determination of NO2 column amounts from AERONET data ,'' *Izv. Atmos. Oceanic Phys.* **40**, 54–67 (2004).

**Nickolay Krotkov** received his BS in physics and MS degree in remote sensing in 1985 from the Moscow Institute of Physics and Technology, Russia. He received his PhD in oceanography (physics and mathematics) in 1990 from the P. P. Shirshov Institute of Oceanology, Russian Academy of Sciences, for research on using polarization properties of light in oceanic remote sensing. He joined NASA, Goddard Space Flight Center, in 1993 where he worked on applications of satellite data, such as mapping surface UV irradiance and generation of UV volcanic eruption data products from the NASA Total Ozone Mapping Spectrometer (TOMS) missions. His main field of research is radiative transfer modeling, satellite and ground based UV data analysis, and inversions. He is currently a senior research scientist with GEST Center University of Maryland Baltimore County.

**Pawan K. Bhartia** received his PhD in physics and MS degree in computer science in 1977 from Purdue University, West Lafayette, Indiana. Since then he has been associated with NASA's Goddard Space Flight Center (GSFC) in Greenbelt, Maryland. Between 1977 and 1991 he worked with several private companies, including Systems and Applied Sciences Corporation, STX, SAR, Interferometrics, and TRW on NASA contracts. Since October 1991 he has been a NASA employee. Currently he is the head of the Atmospheric Chemistry and Dynamics Branch at GSFC. He is also the project scientist of NASA's Total Ozone Mapping Spectrometer (TOMS) satellite mission and the U.S. science team leader of the Ozone Monitoring Instrument (OMI)—a joint project between NASA and The Netherlands. He has over 50 publications in UV remote sensing of the Earth from satellites, dealing principally with the measurement of the Earth's ozone layer. He is a member of the American Geophysical Union.

**Jay Herman** received his BS degree in 1959 from Clarkson, and MS in 1963 and PhD in 1965 in physics and aeronomy from Pennsylvania State University. He joined NASA, Goddard Space Flight Center, first with a National Academy of Sciences postdoctoral appointment and then as a staff scientist. He has worked in a number of fields including chemical modeling of the Earth and planetary atmospheres, radiative transfer, satellite data studies of ozone, clouds, surface reflectivity, and UV radiation in the atmosphere and oceans. He currently is project scientist on the Deep Space Climate Observatory at the Lagrange-1 observing point. He is also principal investigator on the Earth UV radiation project. He is a long-term member of the American Geophysical Union.

**James Slusser** studied physics at Western Michigan University and received his bachelor's degree in 1977 and his master's degree in 1980. The next nine years were spent in Chicago, Illinois, where he was the undergraduate physics laboratory director at Loyola University. Later he worked as a design engineer for Atlas Electric Devices, serving as a project manager for an ultraviolet outdoor radiometer and temperature probe for weathering chambers. In 1989 he returned to school to study atmospheric science and radiative transfer at the University of Alaska at Fairbanks. His dissertation involved measuring stratospheric nitrogen dioxide and exploring its relationship to ozone abundances. After earning his PhD in 1994 he spent three months at Lauder, New Zealand doing trace gases analysis using the zenith sky spectroscopy. He then took up a position as a research associate at the Center for Atmospheric Science at Cambridge University in England where he investigated the effects of volcanic aerosols on nitrogen dioxide and ozone abundances in Antarctica. In 1996 he became a research scientist at the USDA UV-B Monitoring and Research Program at Colorado State University, and in 1999 he became program director. His current research interests include improving the calibration accuracy and precision of UV measurements and retrievals of trace gas column abundances and aerosol properties. He has authored or co-authored more than 25 papers. He is a member of the AGU, AMS, and SPIE, and served as an associate editor of the *Journal of Geophysical Research*.

**Gwendolyn Scott** received her BA degree in biology (with a chemistry minor) from the University of Evansville in 1971, and her BS degree in computer science from Colorado State University (CSU) in 1998. She has been employed at CSU's Natural Resource Ecology Laboratory for 26 years: in the laboratory, performing chemical analyses from 1974 to 1982; in data management for the National Atmospheric Deposition Program (NADP) from 1983 to 1994; and, in software development for the USDA UV-B Monitoring and Research Program since 1998.

**Gordon Labow** received his BS degree from Virginia Tech in 1986 and joined NASA's Goddard Space Flight Center Solar Maximum Mission team that same year. He worked on increasing our understanding of the processes that create solar flares and methods of flare prediction. In 1992 he began to work with the Total Ozone Mapping Spectrometer (TOMS) team and has experience with the instrumentation and algorithmic methods used for detection of ozone, as well as the statistical techniques used for the calculation of ozone trends. He has experience working on ground-based instrumentation, such as spectrometers, radiometers, ozonesondes, and others used to detect trace gases such as ozone, $SO_2$, $NO_2$ as well as aerosols. He is currently a senior scientist with Science Systems & Applications Inc. of Lanham, Maryland.

**Alexander Vasilkov** received his MS degree in aerospace engineering and PhD in physics and mathematics from the Moscow Institute of Physics and Technology in 1971 and 1975, respectively. His research interests are in the areas of radiative transfer of solar radiation in the atmosphere-ocean system and development of algorithms for retrieving seawater bio-optical parameters from satellite measurements of spectral reflectance. In 1980s, he was first to develop a polarization technique for airborne lidar sensing of the vertical profile of seawater turbidity. Currently, he is working on the development of a cloud pressure algorithm based on Raman scattering in the atmosphere and ocean.

**Thomas F. Eck** received his BS degree in meteorology from Rutgers University in 1977 and his MS degree in meteorology from the University of Maryland, College Park, in 1982 where his major interests were in micrometeorology and remote sensing. In 1981 be began work at Goddard Space Flight Center and has continued through to the present. He is currently a research scientist with the GEST Center, University of Maryland, Baltimore County, where he carries out instrument calibration and deployment, field experimentation, data analysis, and scientific research within the global Aerosol Robotic Network (AERONET) project. He has authored and co-authored over 65 papers with recent emphasis on studies of the optical properties of atmospheric aerosols, especially from biomass burning and fossil fuel combustion, and the attenuation of solar flux by aerosols.

**Oleg Dubovik** received his BS and MS degrees in 1985 in physics (optics) from the Belarus State University, Minsk. He received his PhD in physics and mathematics from the Institute of Physics, Minsk, in 1992. Starting from 1985 he began his research experience at Institute of Physics, employed first as assistant research staff member and later as a research scientist. In the period from 1995 to 1997, Dr. Dubovik worked at the National Institute for Environmental Studies, Tsukuba, Japan, as visiting scientist supporting an ILAS/ADEOS project. Since April 1997, Dr. Dubovik has been working at GSFC as a contractor. During his career he has been involved in developing and implementing inversion algorithms for aerosol optical properties from measurements of atmospheric radiation.

**Brent Holben** received his MS degree from Colorado State University, Fort Collins, in 1976, specializing in biometeorology and remote sensing. He is currently a research scientist at NASA's Goddard Space Flight Center, Greenbelt, Maryland. He was a staff scientist with the University of Puerto Rico/Puerto Rico Nuclear Center investigating mesoscale radiation balance in the Luquillo Experimental Forest until 1978 when he joined the GSFC. He has published research on remote sensing of vegetation dynamics, atmospheric corrections to remotely sensed data, and more recently, aerosol optical properties. He is the project leader of the ground-based aerosol characterization program AERONET, initiating and guiding its development since 1992.